An Analysis of W-fibers and W-type Fiber Polarizers

Corey M. Paye

Thesis submitted to the Faculty of the Virginia Polytechnic Institute and State University
in partial fulfillment of the requirements for the degree of

Master of Science
in
Electrical Engineering

Roger Stolen, Chair
Ira Jacobs
Ahmad Saafai-Jazi

April 27, 2001
Blacksburg, Virginia

Keywords: Fiber optics, optical fibers, W-fibers, Fiber polarizers

Copyright 2001, Corey M. Paye

An Analysis of W-fibers and W-type Fiber Polarizers

Corey Paye

(Abstract)

Optical fibers provide the means for transmitting large amounts of data from one place to another and are used in high precision sensors. It is important to have a good understanding of the fundamental properties of these devices to continue to improve their applications.

A specially type of optical fiber known as a W-fiber has some desirable properties and unique characteristics not found in matched-cladding fibers. A properly designed W-fiber supports a fundamental mode with a finite cutoff wavelength. At discrete wavelengths longer than cutoff, the fundamental mode experiences large amounts of loss. The mechanism for loss can be described in terms of interaction between the fiber's supermodes and the lossy interface at the fiber's surface. Experiments and computer simulations support this model of W-fibers.

The property of a finite cutoff wavelength can be used to develop various fiber devices. Under consideration here is the fiber polarizer. The fiber polarizer produces an output that is linearly polarized along one of the fiber's principal axes. Some of the polarizer properties can be understood from the study of W-fibers.

Acknowledgements

The author would like to acknowledge the continuous guidance, support and understanding provided by his parents. They have made many of life's achievements possible.

I would also like to acknowledge the patience and support of my advisor, Dr. Roger Stolen. I would like to thank him for giving me the opportunity to work with him.

Table of Contents

Table of Figures

Chapter 1:

Introduction

When John Tyndall used a thin stream of water to guide light in 1870 [1], he demonstrated the important fact that light can be controlled and channeled. Over the past several decades, many different lightguides have been developed. Arguably, the best medium or channel along which light signals can propagate is the glass optical fiber. The properties of the optical fiber allow the information encoded in light pulses to travel hundreds of kilometers without being lost due to undesirable effects such as signal attenuation or chromatic dispersion.

Optical fibers have become the backbone of the information age. Every day gigabits of information crisscross the globe on fiber optics. A clear understanding of the fundamental properties of fibers is needed to not only support the current optical networks in place, but to also ensure the development of more powerful networks in the future. An understanding of fiber optics is also important for the development of the fiber components found not only in communication systems but also in the many types of fiber sensors.

In 1983, several members of Bell Telephone Laboratories published a paper describing a flattened, elliptical, single-polarization fiber [2]. Over a range of wavelengths, these single-polarization fibers allow light to propagate along only one axis of the fiber. That is, over a certain wavelength range, unpolarized light injected into the single-polarization fiber will emerge linearly polarized along a principal axis at the output.

These single-polarization fibers use a combination of a depressed cladding (DC) refractive index profile and purposely-induced high birefringence that defines two distinct orthogonal axes within the fiber. The induced birefringence lies along the major and minor axes of the elliptical fiber. The induced birefringence is much stronger than any birefringence caused by bending, thermal fluctuations, or other mechanisms. The effect of the high birefringence is to cause each axis to have a different refractive index profile along the length of the fiber. A fiber with a DC structure (which consists of a core, inner cladding and outer cladding) can be designed such that the fundamental mode

of the fiber experiences a non-zero cutoff wavelength [3]. When this occurs, the mode field is no longer truly guided by the fiber and can experience a high amount of loss. In the single polarization fiber, the high birefringence causes a different cutoff wavelength of the fundamental mode along each principal axis. That is, a combination of a DC structure with high birefringence allows differential attenuation of light along each principal axis of the fiber. These single-polarization fibers can be used in coherent communication systems, high-precision sensors, fiber gyroscopes, and in-line fiber amplifiers [4] [5] [6].

The mechanisms at work within this type of polarizer fiber are not completely understood. Attempts to fully characterize these fibers so far have been unsuccessful. Even though many samples of single polarization fibers with similar structures were made from different preforms at Bell Labs, there does not seem to be a clear connection between variations in the fiber parameters and their resultant effects. Some of the difficulty in understanding the polarizers comes from the unique shape of the fibers: a roughly circular core is surrounded by a thin elliptical inner cladding, which in turn is surrounded by one or two elliptical outer claddings. The outermost cladding is flat along two sides giving the fiber a slab-like structure in this region. More significantly though, there is a lack of a full understanding of the properties of DC fibers (also referred to as W-fibers). Many previous investigations of W-fibers did not consider what happens beyond fundamental mode cutoff. In the polarizer fibers, this is the most important region of operation to consider since this is the region in which the fiber operates with a single polarization.

The purpose of this thesis is to present data from experiments and computer simulations that will help explain the characteristics of W-fibers and the operation of the fiber polarizers. The analysis of the data will also try to explain the different mechanisms at work within the fibers.

This paper is divided into five chapters. Chapter 2 briefly reviews the general analysis of optical fibers. Starting with Maxwell's equations, the homogeneous vector wave equations are derived. These are used in an analysis of a fiber with an arbitrary index profile and number of layers.

Chapter 3 covers the modal analysis and characteristics of W-fibers. This chapter starts with the application of general fiber analysis to the analysis of W-fibers. Next there is a discussion of what happens when the cutoff wavelength is reached and the disagreement between theoretical predictions and experimental data. Two models are presented to describe W-fiber properties. Data from experiments and computer simulations are used to fully develop one of the models to comprehensively describe W-fiber characteristics.

Chapter 4 discusses the single-polarization fiber. This chapter begins by clearly defining what is meant by a single-polarization fiber and presenting examples of its design and index profiles. Next, the principals of how these fibers work is discussed. To do this, the concept of birefringence will be explained with some detail along with an explanation of cutoff in connection to the polarizers. Next problems in understanding the polarizer are explained. Finally, some experimental results are presented to help determine how the polarizers can be improved.

Finally, Chapter 5 lists suggestions for further experimentation. This last chapter will also discuss some of the potential applications of the single-polarization fiber.

Chapter 2:

Analysis of EM Wave Propagation in Optical Fibers

This chapter investigates the propagation of electromagnetic (EM) waves in optical fibers. The first section shows the derivation of the wave equations used in optical waveguide analysis. Next, these wave equations are used to analyze an optical fiber with an arbitrary refractive index profile and an arbitrary number of layers. The approximations and assumptions made in carrying out waveguide analysis are listed and validated. The assumptions used in this chapter will be used throughout the rest of this thesis.

2.1 Approach to Waveguide Analysis

The analysis of dielectric waveguides begins with Maxwell's equations. Using the Cartesian coordinate system (x, y, z) and assuming a dependence on frequency (rather than time) the time harmonic Maxwell's equations are defined as:

$$\nabla \mathbf{x}\mathbf{E} = -j\omega\mathbf{B} = -j\omega\mu_o\mathbf{H} \tag{2.1a}$$

$$\nabla \mathbf{x}\mathbf{H} = j\omega\mathbf{D} = j\omega\varepsilon\mathbf{E} \tag{2.1b}$$

$$\nabla \bullet \mathbf{D} = 0 \tag{2.1c}$$

$$\nabla \bullet \mathbf{B} = 0 \tag{2.1d}$$

In equations 2.1a through 2.1d, **E** is the electric field, **H** is the magnetic field, **D** is the electric flux density, **B** is magnetic flux density, μ_o is the permeability of free space, and ε is the material permittivity. The radian frequency of the wave, ω, is defined as $\omega = 2\pi f$, where f is the frequency of the wave in Hertz. All quantities indicated in bold are vectors. The time harmonic equations are used because in optical systems, the EM waves are generated by a laser source which ideally operates at a single frequency.

Equations 2.1a – 2.1d do not represent the full Maxwell's equations, but reflect some of the simplifications made when analyzing dielectric waveguides. First, it is understood that since the waveguide is non-magnetic, the relative permeability, μ_r, is

equal to one. Thus, the material permeability, $\mu = \mu_r * \mu_o$, is simply μ_o. Next, since the material does not contain any charge sources, equation 2.1c is set equal to zero.

Since the **E** and **H** fields are usually the quantities of interest, they need to be decoupled so independent equations can be formed. By applying the vector identity:

$$\nabla \mathbf{x} \nabla \mathbf{x} \mathbf{A} = \nabla(\nabla \bullet \mathbf{A}) - \nabla^2 \mathbf{A}$$

equations 2.1a and 2.1b are decoupled into:

$$\nabla^2 \mathbf{E} + k_o^2 n^2 \mathbf{E} = -\nabla\left[\frac{\nabla \bullet n^2}{n^2}\mathbf{E}\right] \tag{2.2a}$$

$$\nabla^2 \mathbf{H} + k_o^2 n^2 \mathbf{H} = -\left(\frac{\nabla \varepsilon}{\varepsilon}\right) x (\nabla x \mathbf{H}) \tag{2.2b}$$

The above equations are known as the inhomogeneous vector wave equations for the **E** and **H** fields. In these equations, k_o is the free space wavenumber defined as $2\pi/\lambda$, where λ is the wavelength of the field. The refractive index of the material, n, is related to the material permittivity by:

$$\varepsilon = \varepsilon_o \varepsilon_r = \varepsilon_o n^2 \tag{2.3}$$

where ε_o is the permittivity of free space and ε_r is the dielectric constant of the material. In general, n and ε_r are not constant but are a function of position within the waveguide. This is because practical optical fibers consist of multiple layers with different refractive index values.

At this point, a practical consideration is used to greatly simplify the vector wave equations. In practical optical fibers, the layers of glass have approximately equal refractive index values. There are several reasons for this. First, materials with very different index values will have different thermal expansion coefficients. Therefore, if the index difference between layers is too large, changes in the ambient temperature in the fiber's environment will cause stress at the interface between layers and can cause

defects in the fiber. Another reason to keep the index difference between layers small is to ensure that the fiber is single-moded at typical operating wavelengths (850 – 1550 nm) and at the same time have a workable core size. The wavelength at which a fiber becomes single-moded is a function of the core radius and the difference in refractive indices of the core and cladding. Typically, the difference in the refractive index between each layer is less than 1%. Thus, since n changes only very slightly over the cross section of the fiber, its derivative can be approximated as zero and therefore the derivative of ε in Equation 2.2 can be approximated as zero. By examining the right hand side of equations 2.2a and 2.2b and noting that ∇is the partial derivative with respect to x, y or z, it can be seen that the vector wave equations can be approximated as homogeneous differential equations:

$$\nabla^2 \mathbf{E} + k^2 n^2 \mathbf{E} \approx 0 \qquad (2.4a)$$

$$\nabla^2 \mathbf{H} + k^2 n^2 \mathbf{H} \approx 0 \qquad (2.4b)$$

The above equations are referred to as the homogeneous vector wave equations of **E** and **H**. Since the **E** and **H** fields are comprised of three components each (i.e. x, y and z) these equations actually represent six scalar wave equations. The next section will show that with some approximations, the full vector wave equations are not always necessary for waveguide analysis. In many cases, scalar analysis of waveguides is sufficient.

2.2 Scalar Wave Analysis of Multiple Layer Dielectric Waveguides

The homogeneous vector wave equations are the starting point for the next step in the analysis of dielectric waveguides. One of the main objectives in the analysis of optical waveguides is to derive a set of expressions that describe the EM fields in the different layers of the waveguide. The field expressions are then used to determine the propagation constant of the different modes of the waveguide.

The general system under consideration is a multiple layer, circularly symmetric, dielectric waveguide with an arbitrary index profile. Figure 2.1 is a cross section of this system. The refractive index of each layer is designated n_1, n_2, n_3, ..., n_i and a_1, a_2, a_3, ...,

a_i are the radii of each layer. It is assumed that the direction of propagation of the EM field is in the positive z direction.

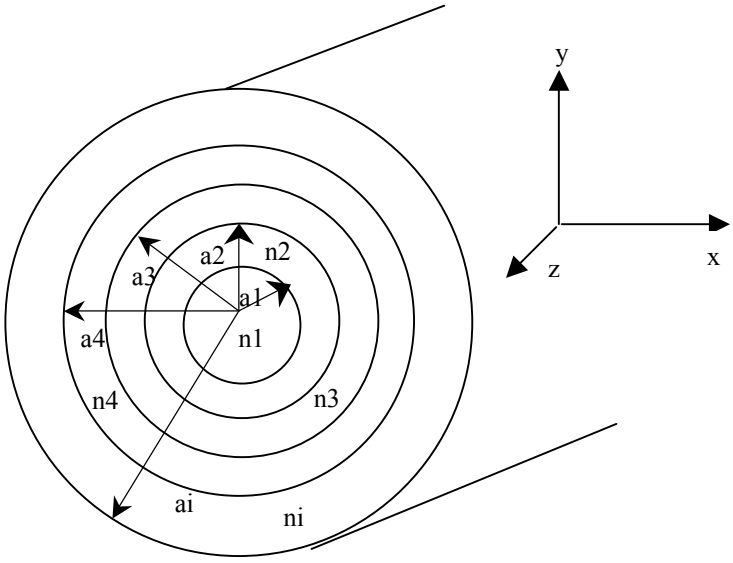

Figure 2.1: Cross-sectional end view of an optical fiber with an arbitrary number of layers.

The following assumptions are made in the analysis of the above waveguide:

1. The waveguide is straight and infinitely long
2. The waveguide is lossless
3. The effect of non-linearities can be ignored
4. The outermost layer extends to infinity

The first assumption means that the fiber is free from any perturbations such as bends or twists that can cause an asymmetry in the index profile of the fiber. Methods exist for the analysis of asymmetric waveguides, however it is sufficient to assume that the perturbations are weak enough that they will not affect the fiber's behavior. By assuming an infinitely long waveguide, the effects of the discontinuities at the fiber end faces are neglected. The second assumption that the waveguide is lossless means that the modal propagation constants are real. The lossless assumption is reasonable since many contemporary fibers can have losses as low as 0.2 dB/km [7]. Non-linearities in optical fibers arise because of the material's response to intense EM fields [7]. Non-linearities can be a serious consideration in SM fibers where the mode power is tightly confined to

the core and thus a strong field is focused into a small area. They are also a concern in long-distance telecommunications applications where large amounts of power are launched into the fiber to maximize the allowable repeater or amplifier spacing. However non-linear effects are relatively weak at low powers and the data collected for this thesis was from probing fibers using very low-power sources, therefore the non-linear effects will be neglected in the waveguide analysis. The last assumption of an infinite cladding is used because the EM field within a SM fiber decays rapidly outside of the core and therefore the outer region acts as an infinite medium. However, later sections will show that the assumption of an infinite outer cladding is not always accurate in the analysis of some waveguides.

The techniques used to analyze the type of structure shown in Figure 2.1 are well established in many sources such as Agrawal [7]. Therefore, for the sake of brevity, the general formalism is only summarized here.

The system under consideration lends itself to analysis using cylindrical coordinates, (r, ϕ, z). The homogeneous vector wave equations for the **E** and **H** fields (2.4a and 2.4b), can be rewritten in cylindrical coordinates as:

$$\frac{\partial^2}{\partial r^2}\boldsymbol{\psi} + \frac{1}{r}\frac{\partial}{\partial r}\boldsymbol{\psi} + \frac{1}{r^2}\frac{\partial^2}{\partial \phi^2}\boldsymbol{\psi} + q^2\boldsymbol{\psi} = 0 \qquad (2.5)$$

where $q^2 = (k^2n^2 - \beta^2)$, n is the refractive index of the material and $\boldsymbol{\psi}$ can represent either the $\mathbf{E}_x$, $\mathbf{E}_y$, $\mathbf{E}_z$, $\mathbf{H}_x$, $\mathbf{H}_y$ or the $\mathbf{H}_z$ field. It is assumed that the **E** and **H** fields propagate in the positive z-direction and have the form: $\psi = \psi(r,\phi)\exp(-j\beta z)$. The term β is referred to as the modal propagation constant.

Since both of the vector fields (**E** and **H**) consist of three components ($\{e_r, e_\phi, e_z\}$ and $\{h_r, h_\phi, h_z\}$) the vector wave equation actually represents six separate equations. The type of mode under analysis determines which of the six scalar equations are used. The modes of a circularly symmetric fiber are classified into transverse electric (TE) transverse magnetic (TM) and hybrid modes (EH or HE). TE modes consist of the (h_r, e_ϕ, h_z) fields, TM modes consist of the (e_r, h_ϕ, e_z), and hybrid modes consist of all six fields.

Therefore, when analyzing waveguides that have more than a few layers using the full vector equations can quickly become very complicated.

A set of assumptions greatly simplifies the work of analyzing waveguides [9]. The assumptions state that since the refractive indices of each layer of the fiber are nearly equal, the modes of the fiber are "weakly guided". In this approximation, the longitudinal field components (e_z and h_z) are very small compared to the transverse components (e_r, e_ϕ, h_r, h_ϕ) and therefore can be neglected. "Similar" modes (e.g. TE_{om}, TM_{om}, HE_{2m}) are nearly degenerate (i.e. they have nearly the same propagation constants). These nearly degenerate modes are grouped together and designated as "linearly polarized" (LP) modes. The LP modes are a superposition of several modes and are linearly polarized along one of the fiber's principal axes. The notation for LP modes is: LP_{mn}, where m is the order of the mode and n is the number of the mode. The subscripts m and n are both integers; m is greater than or equal to zero and n is greater than or equal to one. In optical fibers LP_{01} is the fundamental mode, LP_{11} is the next highest mode and so on. In the weakly guiding approximation, the term "ψ" now simply represents the total field polarized along one of the fiber's principal axes rather than one of the separate components of the **E** or **H** fields. The type of analysis based on the weakly guiding approximation is known as the scalar wave analysis and is the analytical method used in this thesis.

Under the weakly guiding approximation, equation 2.5 remains the same, but is referred to as the scalar cylindrical wave equation and the vector term $\boldsymbol{\psi}$ becomes a scalar quantity. The solution to the scalar cylindrical wave equation consists of the regular and modified Bessel functions (J, Y, and I, K respectively). Using the notation shown in Figure 2.1, Equations 2.7 (a – f) show how these Bessel functions are used to define the EM field across the fiber's cross section.

$$\psi = \begin{cases} A_1 Z_m(u_1 r / a_1) & 0 < r < a_1 \quad (2.6a) \\ A_N Z_m(u_N r / a_N) + \mathbf{A}_N \tilde{Z}_m(u_N r / a_N) & a_{N-1} < r < a_N;\ \ N = 2,3,...i-1 \quad (2.6b) \\ A_i K_m(u_i r / a_i) & r > a_i \quad (2.6c) \end{cases}$$

$$Z_m = \begin{cases} J_m & if\ \underline{n} < n_i \\ I_m & if\ \underline{n} > n_i \end{cases} \tag{2.6d}$$

$$\tilde{Z}_m = \begin{cases} Y_m & if\ \underline{n} < n_i \\ K_m & if\ \underline{n} > n_i \end{cases} \tag{2.6e}$$

$$u_i = a_i \sqrt{|\, n_i^2 k^2 - \beta^2 \,|} \tag{2.6f}$$

In equations 2.6d – 2.6f, $\underline{n}$ is the mode effective index, m is the order of the mode under consideration and A_1, A_N, $\mathbf{A}_N$, and Ai are constant coefficients. The value of the modal propagation constant, β, uniquely defines a mode. It is related to the mode effective index by $\beta = k*\underline{n}$.

Fiber mode fields must be continuous and bounded. Thus in the core ($0 < r < a_1$) the Y and K functions are omitted because they are unbounded when their argument approaches zero. In the outer cladding ($r > a_i$), the I Bessel function is omitted because it becomes unbounded when its argument approaches infinity. The solution shown in equations 2.6a – 2.6c is for truly guided modes (i.e. the field decays in an exponential fashion in the outermost layer of the fiber). The fields in these equations are shown only for $r > 0$ because of the symmetry of the waveguide (i.e. because the fiber is circularly symmetric, the field for $r < 0$ is the same as $r > 0$). It has been assumed that the index within each layer is uniform.

The framework is now set for applying the solutions for the scalar wave equation to a specific system. The next chapter uses the scalar analysis to find the modal propagation constants in a W-fiber. This in turn will help in the understanding of this particular type of optical fiber.

Chapter 3:

Analysis of W-fibers

This chapter discusses the analysis of a specific kind of fiber: the depressed inner cladding fiber, also known as the W-fiber. The technique for the mathematical analysis of an optical fiber with arbitrary parameters introduced in the previous chapter is applied to the W-fiber in this chapter.

This chapter is divided into six sections. The first section briefly gives some background on W-fibers. The main purpose is to establish vocabulary and some of the basic properties of W-fibers. The next section applies the scalar wave analysis to W-fibers and derives the characteristic equation used to find modal propagation constants. The third section closely examines the cutoff of the fundamental mode at a finite wavelength. The section starts by understanding mathematically what happens when the cutoff wavelength is approached. It then describes what happens to the fundamental mode once the cutoff wavelength is exceeded. This description is based on the assumption that the fiber has an infinite diameter. The fourth section presents experimental evidence supporting the hypothesis that beyond the cutoff wavelength, the finite size of the W-fiber plays a role in the fiber's characteristics beyond cutoff. The fifth section presents two different models to explain the anomalous behavior of W-fibers when they are operated beyond the cutoff wavelength. The last section describes some applications of W-fibers.

3.1 W-fiber Background

The general refractive index of a W-fiber is shown in Figure 3.1. In this figure n1, n2, and n3 refer to the refractive indices of the core, inner cladding and outer cladding respectively. The core radius is designated as a, the inner cladding radius as b, and the outer cladding is assumed to be infinite. As mentioned in the previous chapter, the assumption that the outer cladding is infinite is done to simplify the mathematical analysis. Later sections show that in actuality, the size of the W-fiber's outer cladding does affect its characteristics in some cases.

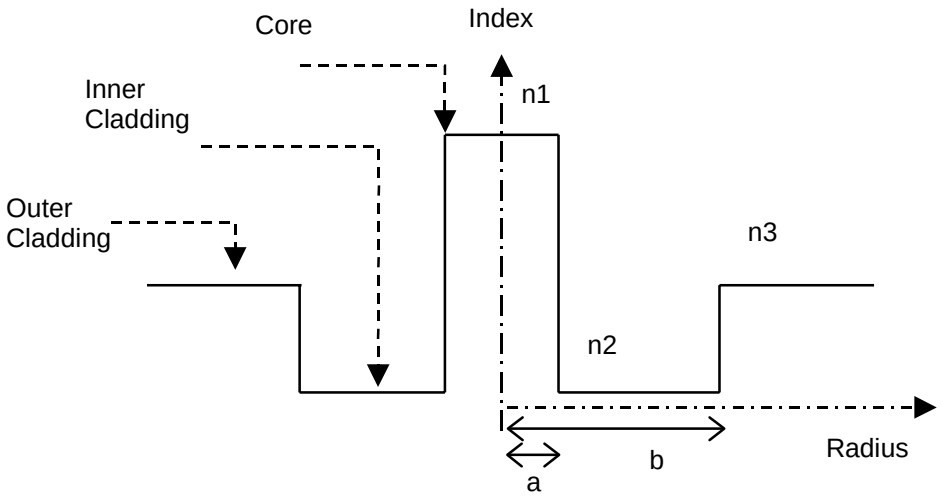

Figure 3.1: Refractive index profile of a W-fiber.

Optical fibers with this type of structure have some interesting properties that are very different from the properties of conventional two-layer fibers (i.e. fibers consisting of only a core and cladding). The properties listed below were first described by Kawakami in 1974 [3]:

1. W-fibers can be designed to have anomalous dispersion in the single-mode frequency region.
2. Single-mode operation in W-fibers can be maintained over relatively large core sizes.
3. In the single-mode regime, in comparison with standard SM fibers, the W-fiber's fundamental mode is more tightly confined within the core of the fiber.
4. W-fibers can be designed so that the fundamental mode will experience cutoff at a finite wavelength.

Several papers have theoretically explained and proven these properties ([10], [11]). However, the first three W-fiber characteristics are listed to give a complete picture of this type of fiber and they will not be elaborated on in this thesis. The cutoff of the fundamental mode at a finite wavelength is the characteristic of interest.

3.2 Scalar Analysis of W-fibers

The general formalism used in Chapter 2 to analyze fibers with arbitrary design parameters is extended with relative simplicity to the analysis of W-fibers. Using the weakly guiding approximation, the fields within the structure shown in Figure 3.1 are defined as:

$$\psi = \begin{cases} A_1 J_m(u_1 r/a) & r < a \\ A_2 \mathrm{Im}(u_2 r/b) + A_3 K_m(u_2 r/b) & a < r < b \\ A_4 K_m(u_3 r/b) & r > b \end{cases}$$

where J, I and K refer to the usual Bessel and modified Bessel functions and A_1, A_2, A_3, and A_4 are the field amplitude coefficients. The mode parameters u1, u2, and u3 are defined as:

$$u_1 = a\sqrt{k^2 n_1^2 - \beta^2} \tag{3.2a}$$

$$u_2 = b\sqrt{\beta^2 - k^2 n_2^2} \tag{3.2b}$$

$$u_3 = b\sqrt{\beta^2 - k^2 n_3^2} \tag{3.2c}$$

For a mode to be a truly guided mode in a W-fiber, its effective index must be between n_1 and n_3. The set of equations shown in equation 3.1 are applicable when the operating wavelength is below cutoff (i.e. $\lambda < \lambda_c$). The case when the operating wavelength is equal to or greater than the cutoff wavelength is treated in the next section.

By requiring the continuity of the field and its radial derivative across each fiber boundary, a set of four equations with four unknowns is generated. This set of equations is used to determine the eigenvalue equation that is used to find the propagation constant of different fiber modes. The eigenvalue equation is found by placing the set of four equations into the following form:

$$\begin{bmatrix} J_m(u_1) & \mathrm{Im}(u_2 s) & K_m(u_2 s) & 0 \\ J_m'(u_1) & I_m'(u_2 s) & K_m'(u_2 s) & 0 \\ 0 & \mathrm{Im}(u_2) & K_m(u_2) & K_m(u_3) \\ 0 & u_2 I_m'(u_2) & u_2 K_m'(u_2) & u_3 K_m'(u_3) \end{bmatrix} \begin{bmatrix} A_1 \\ A_2 \\ A_3 \\ A_4 \end{bmatrix} = \begin{bmatrix} 0 \\ 0 \\ 0 \\ 0 \end{bmatrix} \tag{3.3}$$

In the above expression, s = a/b, which is the ratio of the core radius to the inner cladding radius. The primed functions indicate derivatives taken with respect to argument of the Bessel function. To avoid a trivial solution, it is required that the determinant of the first matrix be zero.

By finding the determinant of the matrix in equation 3.3, the eigenvalue equation for a W-fiber is [10]:

$$\frac{\left[\hat{J}_m(u_1) - \hat{K}_m(u_2 c)\right]\left[\hat{K}_m(u_3) + \hat{I}_m(u_2)\right]}{\left[\hat{J}_m(u_1) + \hat{I}_m(u_2 c)\right]\left[\hat{K}_m(u_3) - \hat{K}_m(u_2)\right]} = \frac{I_{m+1}(u_2 c) K_{m+1}(u_2)}{I_{m+1}(u_2) K_{m+1}(u_2 c)} \qquad (3.4)$$

where:

$$\hat{Z}_m(x) = \frac{Z_m(x)}{x Z_{m+1}(x)} \qquad (3.4b)$$

and

$$c = \frac{a}{b} = \frac{1}{s}. \qquad (3.4c)$$

(Z in equation 3.4 can represent either the J, I or K Bessel functions). The eigenvalue equation is used to find the propagation constant of the modes of the W-fiber. To do this, two of the mode parameters (u_1, u_2 or u_3) are re-written in terms of the third mode parameter. A numerical computer program is then used to find the value of the third mode parameter that satisfies the equality in equation 3.4. Once the value of a mode parameter is determined, it is simple to find the value of the propagation constant for a particular mode.

Two common parameters used to characterize an optical fiber are the normalized frequency, also referred to as the V-number, and the normalized propagation constant. By plotting the normalized propagation constant versus the V-number for a particular

fiber, it is possible to determine which fiber modes are supported at different wavelengths. Once the geometry of the fiber becomes more complicated than the standard two-layer structure, definitions of these normalized parameters can vary from source to source and therefore can be somewhat arbitrary. The definitions for the normalized frequency and normalized propagation constant used in this thesis are the ones used by Monerie [10]. The normalized frequency (V) is defined as:

$$V = ka\left(n_1^2 - n_3^2\right)^{1/2} \tag{3.5}$$

While the normalized propagation constant (B) is defined as:

$$B = \frac{\beta^2 - k^2 n_3^2}{k^2\left(n_1^2 - n_3^2\right)} \tag{3.6}$$

From the definition of the normalized propagation constant, it can be seen that for guided modes, B will lie between 0 and 1 (i.e. the modal effective indices will be between n_1 and n_3).

Figures 3.2a and 3.2b show the variation in B with respect to V for the LP01 mode in a W-fiber. Data points in each figure were calculated using different ratios of b/a and the different curves in each figure are for a different ratio of Δn'/Δn. The proportion b/a is the ratio of the inner cladding radius to the core radius. The terms in the ratio Δn'/Δn are defined as [10]:

$$\Delta n' = n_2 - n_3 \tag{3.7a}$$

$$\Delta n = n_1 - n_2 \tag{3.7b}$$

From the index profile of the W-fiber (Figure 3.1) it is clear that the ratio of Δn'/Δn will always be negative. Also included in Figures 3.2a and 3.2b is the B vs. V curve for a standard step-index SM fiber (i.e. a fiber without a depressed cladding). This curve is referred to as the "standard" curve in each figure.

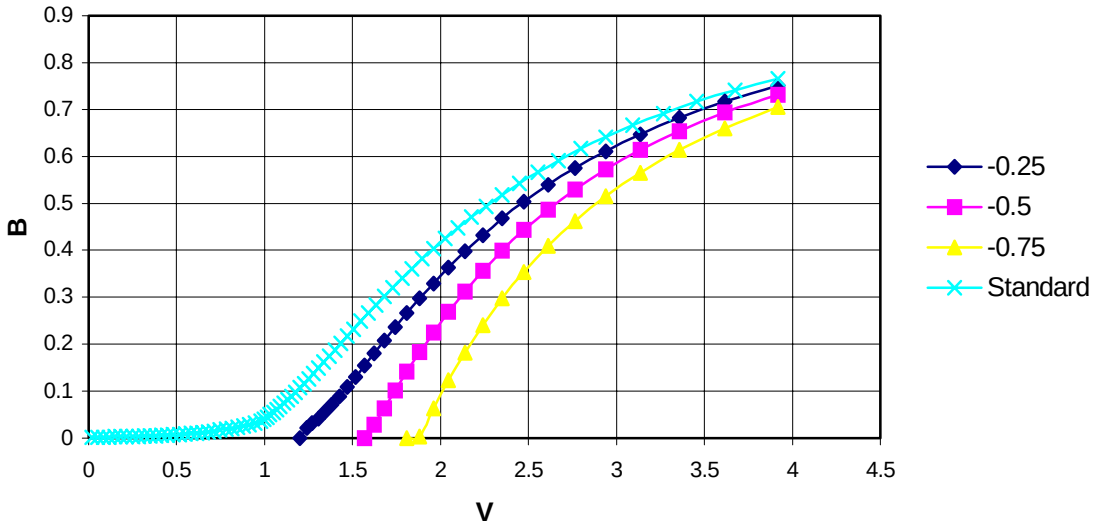

Figure 3.2a: Plot of normalized propagation constant versus normalized frequency (b/a =).

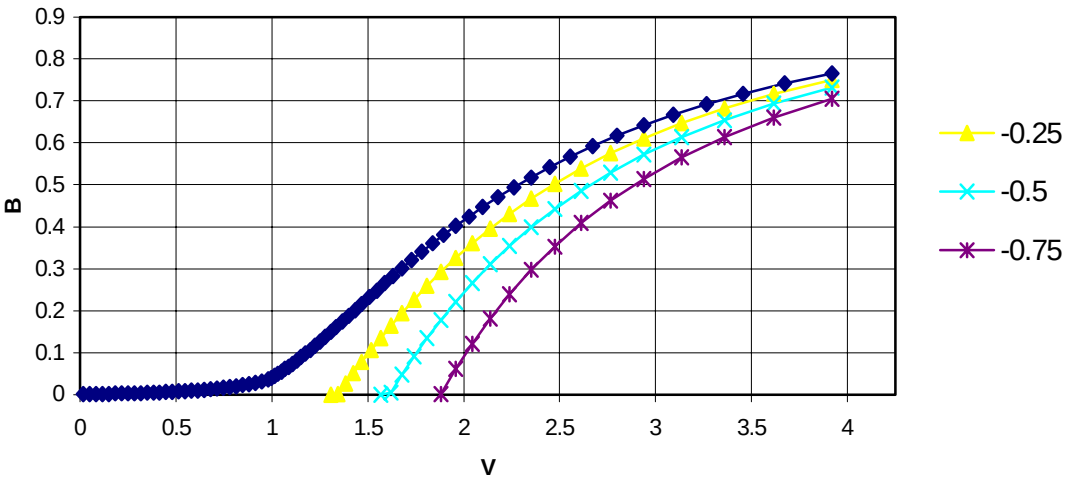

Figure 3.2b: Plot of normalized propagation constant versus normalized frequency (b/a = 5).

The above curves were generated using a MATLAB simulation program and are in good agreement with published results [10]. This computer program is discussed in more detail later in the chapter.

Several pertinent pieces of information can be extracted from Figures 3.2a and 3.2b. First, the curves for the W-fiber reach a value of B = 0 for a non-zero value of V, while the curve for the standard fiber reaches B = 0 only when V = 0. From equation 3.5 it can be seen that V = 0 only when the wavelength approaches infinity. Therefore, a properly designed W-fiber can reach cutoff at a finite wavelength (the necessities of this proper design are discussed in the next section). Second, as expected, it can be seen that as the ratio of $\Delta n'/\Delta n$ becomes smaller (more negative) the fundamental mode in a W-fiber will reach cutoff at a shorter wavelength. Consider the case when the core and outer cladding indices are fixed. As the wavelength increases (and V decreases), the fundamental mode spreads out further from the core. As the mode spreads, it "sees" more of the depressed region. Therefore, a W-fiber with a lower depression, and hence a more negative $\Delta n'/n$ ratio, will cause the effective index of the fundamental mode to decrease faster with an increase in wavelength. This leads to the conclusion that the value of the cutoff wavelength of the fundamental mode in a W-fiber can be tailored using fiber parameters.

This section demonstrated how the scalar wave analysis is applied to W-fibers. This analysis can be used to find different modal propagation constants and to understand how varying W-fiber parameters affect which modes are supported by the W-fiber at different wavelengths. The next section examines what occurs when the operating wavelength becomes equal to the cutoff wavelength in a W-fiber.

3.3 Cutoff in W-fibers

"Cutoff" in W-fibers refers to the mathematical cutoff of the fundamental mode. At the cutoff wavelength (λ_c), the modal effective index of the fundamental mode is equal to the index of the outer cladding. This section discusses what design parameters are necessary for cutoff to occur, what occurs as the cutoff wavelength is approached, and how power in the fundamental mode is lost beyond cutoff when it is assumed that the outer cladding extends to infinity.

Simply inserting a depressed index region between the core and the outer cladding does not guarantee that the fundamental mode has a finite cutoff wavelength [3]. In fact, many designs of practical telecommunication optical fibers (where a finite cutoff wavelength would likely have a detrimental effect) have a slight index depression between the core and cladding. This is done to improve certain fiber properties. For example, a slight depression improves the fundamental mode's confinement to the core and thus lowers the fiber's bend loss [12].

Using the rigorous vector wave analysis, the conditions for a finite cutoff wavelength are [10]:

$$b/a >> 1 \tag{3.8a}$$

and

$$|\Delta n'| \approx \Delta n \tag{3.8b}$$

The conditions in equation 3.8 show that the depression in a W-fiber must be wide enough or deep enough to significantly modify the fundamental mode.

When the operating wavelength is equal to or greater than the cutoff wavelength, the solution to the scalar wave equation shows that the mode field in the W-fiber's outer cladding no longer exponentially decays. Based on the analysis in section 3.2, if the effective index of the W-fiber's fundamental mode is less than n_3, the field in the outer cladding is defined as:

$$\psi = B_1 H_m^2(u_3' r/b) \tag{3.9a}$$

where B_1 is the amplitude coefficients, H_m is the Hankel function and

$$u_3' = b\sqrt{k^2 n_3^2 - \beta^2} \tag{3.9b}$$

Equation 3.9 shows that beyond the cutoff wavelength, the fundamental mode is no longer tightly confined to the core, but forms a radial traveling wave in the outer

cladding. When a W-fiber is operated at wavelengths longer than λ_c the fundamental mode is not considered to be a "truly guided" mode, but it is possible to transmit power from one end of the fiber to the other with relatively low-loss [12]. (A "truly guided" mode is a mode whose effective index value is in between the value of the core index and the index of the outermost cladding.)

In the original theoretical model of the W-fiber, where it is assumed that the outer cladding is infinite, it is argued that the fundamental mode becomes a leaky wave beyond cutoff [3], (leaky waves or modes are defined as guided modes operating at wavelengths greater than cutoff [13]). Once a mode changes from being a truly guided mode to a leaky mode, it begins to experience loss as it propagates along the fiber. An approximate loss coefficient for a W-fiber operating at wavelengths longer than cutoff is defined as [Cohen, 1982 #6]:

$$2\alpha = C\frac{\gamma\sigma e^{-2\sigma b}}{n_{eff}K_1^2(\gamma a)}$$

where $\gamma = (\beta^2 - n_2^2k^2)^{1/2}$, $\sigma = (n_3k^2 - \beta^2)$, n_{eff} is the mode effective index, and $K_1$is a first order K-Bessel function. The constant C is a function of the indices of the core and claddings and the radius of the core. A plot of this loss coefficient with increasing wavelength shows a loss that monotonically increases with wavelength until the loss is too high for power to be transmitted from one end of the fiber to the other.
Based on the above theoretical model, a plot of a W-fiber's loss versus wavelength for operating wavelengths greater than cutoff should show a smooth monotonically increasing curve. However, the following sections show this is not the case and that operating a W-fiber at wavelengths longer than cutoff presents a more complex situation.

3.4 Evidence of Finite Cladding Effects in W-fibers

To begin this section, a recall is made of the issues concerning W-fibers:

1. The fields and modes in a W-fiber are accurately described using the weakly guiding approximation and scalar wave analysis.

2. If a W-fiber is properly designed, the fundamental mode will experience cutoff at a finite wavelength.
3. As λ_o approaches λ_c, the mode field spreads out of the core and "sees" more of the fiber.
4. Past analysis assumed that with an infinitely large outer cladding, close to and beyond cutoff ($\lambda_o > \lambda_c$), the fundamental mode experiences relatively simple radiation loss that increases with wavelength.

This section discusses some of the inaccuracies of the last statement in the above list. Even though there have been relatively few investigations into what actually occurs beyond the cutoff wavelength, it will be quite clear that the model of simple radiation loss does not accurately describe what happens when a W-fiber is excited at wavelengths beyond cutoff.

While several sources report the theoretical cutoff of the fundamental mode in a W-fiber [3] [10] [11], the first report of the experimental verification of cutoff and the measured spectral response of a W-fiber beyond cutoff is from Sansonetti et al. in 1982 [14]. The publication showed that the W-fiber spectrum of the fundamental mode contains discrete loss peaks that build in strength with increasing wavelength until a wavelength is reached where power can no longer be transmitted from one end of the fiber to the other. This type of response was experimentally verified for this thesis. In Figure 3.3, the spectral response of a 1-meter test W-fiber is shown. The fiber was laid straight and excited with a white-light source. The output intensity from the core was measured using an Anritsu optical spectrum analyzer (OSA). The spectrum in Figure 3.3 shows four distinct loss peaks at 775 nm, 825 nm, 925 nm, and 1075 nm. It is clear that as the wavelength increases, the loss peaks become deeper and wider (the loss peak at 1075 nm can be considered infinitely wide and deep). For this thesis, the wavelength at which power can no longer be transmitted from one end of the fiber to the other (in this case 1075 nm), will be referred to as the extinguish wavelength (λ_e). From this measurement, it is clear that beyond cutoff of the fundamental mode, the W-fiber spectral response is not accurately described by the leaky mode loss model.

Since the radiation model is based on the assumption that the fiber's cladding is infinite, it is important to determine if the anomalous loss peaks are caused by some sort

of finite cladding effect. To determine if this is the case, an index matching experiment was performed. First, the spectral response of a sample W-fiber was measured. The fiber was then stripped of its protective jacket and coated with glycerin. Pure glycerin has a

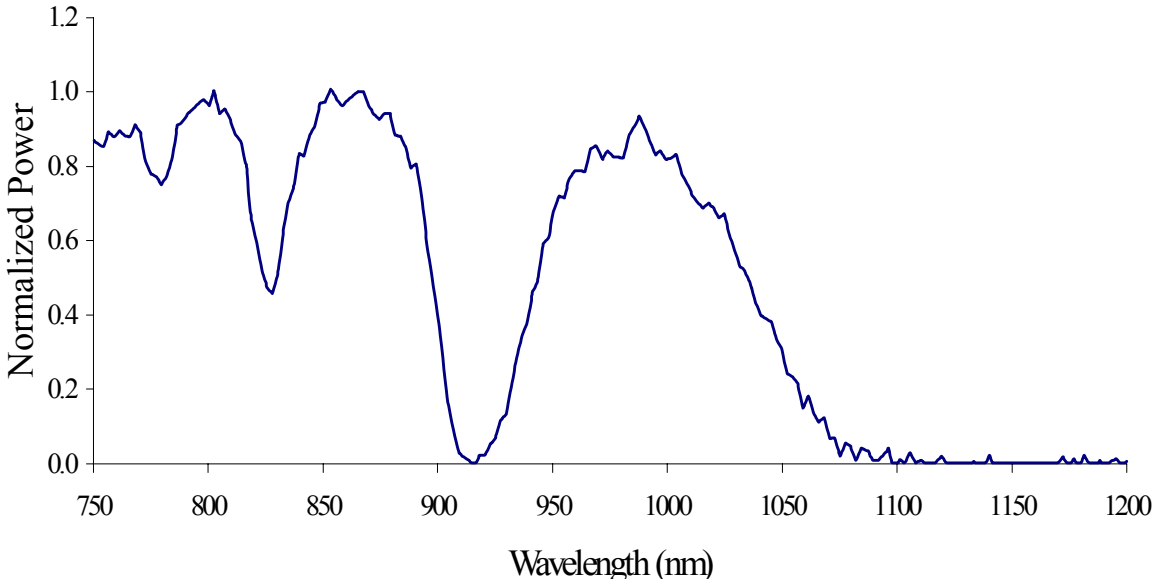

Figure 3.3: Measured spectral response of a 1-meter W-fiber.

refractive index slightly higher than fused silica (the material of the outer cladding in the W-fiber). However, glycerin is highly hygroscopic [15] and as it absorbs moisture from the atmosphere, its refractive index drops. If enough moisture is absorbed, the index of the glycerin closely matches the index of fused silica. This, in effect, simulates an infinite outer cladding. The spectral response of the glycerin coated fiber was then measured. The two spectral responses are shown in Figure 3.4. The spectrum labeled "Original" is spectral response of the jacketed W-fiber. The characteristic loss dips at points "A" and "B" are clearly visible. The measurement of the glycerin coated fiber is labeled "Index Matched". Clearly, the loss peaks are greatly ameliorated when the cladding appears to be infinite. In fact, the matched spectrum closely resembles the sort of spectrum predicted by the simple model of pure radiation loss. That is, the index matched spectrum has very few discernable characteristics except that there is a wavelength after which the system loss is so great that power can not be transferred. It is interesting to note that if the refractive index of the glycerin is much different from the

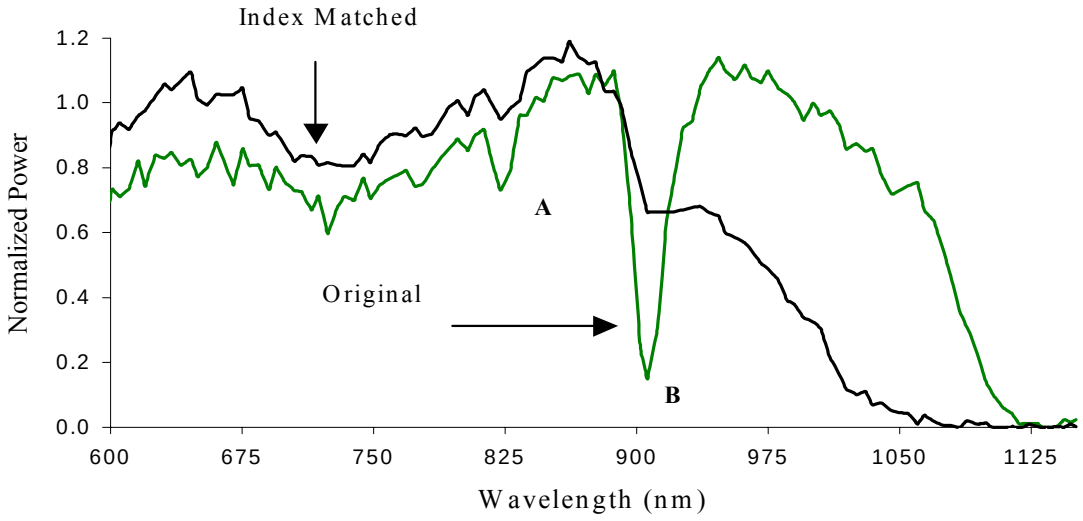

Figure 3.4: Comparison of the spectral response a jacketed W-fiber and an index matched W-fiber.

index of fused silica (either before it absorbs a significant amount of moisture or after it has absorbed too much moisture) it does not affect the W-fiber's spectrum.The above experimental results clearly indicate that simple radiation loss does not accurately describe a W-fiber's response for wavelengths greater than cutoff. It is now important to understand why and how this unexpected behavior comes about.

3.5 W-fiber Models

Since a W-fiber's actual spectral response varies greatly from that predicted by the infinite cladding model, the next step is to develop a new model that accurately describes W-fiber behavior. A few researchers have already developed theories that try to explain the structure found in W-fiber spectral responses [16] [17] [18] [19]. It is felt that these papers are accurate in many respects, but do not fully address all the issues with W-fibers. This section presents two models to explain W-fiber characteristics. The first model uses traditional coupled mode theory. The second model uses the supermode theory, which is believed can explain W-fiber behavior with sufficient accuracy and in much simpler terms.

3.5.1 Mode Coupling Model

A logical first model to develop to describe the W-fiber's spectral characteristics is one based on mode coupling. This is an appealing model to apply to the W-fiber because the discrete loss peaks seen in the W-fiber spectrum are similar to the loss peaks seen in the spectra of long-period fiber gratings that are caused by the fundamental mode coupling to discrete cladding modes. The mode coupling model was first suggested by Francois and Vassallo [16]. Another simpler mode coupling model was also developed by Tomita and Marcuse [20].

The mode coupling model is based on the idea of matching propagation constants of different modes. When the fundamental mode of a W-fiber is excited at

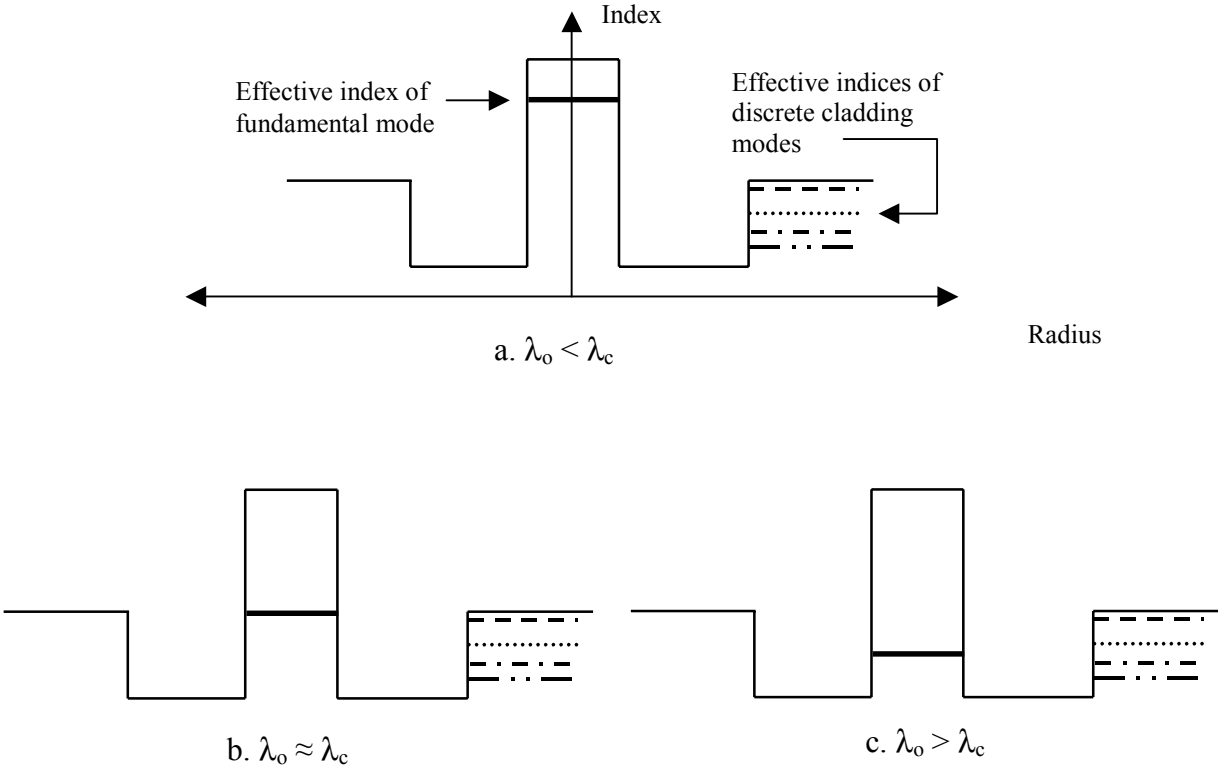

Figure 3.5: Pictorial concept of mode coupling in a W-fiber. a). Operating wavelength is much less than the cutoff wavelength. The fundamental mode is guided and well confined to the core. b) Operating wavelength is slightly less than the cutoff wavelength. The fundamental couples to the lowest cladding mode. c) Operating wavelength is much greater than the cutoff wavelength. The fundamental has coupled to several cladding modes.

wavelengths longer than the cutoff wavelength, its effective index must be less than the index of the outer cladding. At these wavelengths, the propagation constant of the

fundamental mode can become matched to the propagation constant of discrete cladding modes. When the propagation constants of two modes are matched, a significant power transfer from one mode to the other can occur [20]. This concept is depicted schematically in Figure 3.5. In Figure 3.5a, the fundamental mode is a truly bound mode. In this case, the fundamental mode is guided and the modal loss is very small. In Figure 3.5b, the operating wavelength is just slightly greater than the cutoff wavelength, and the effective index of the fundamental mode is equal to the effective index of the first cladding mode. At this wavelength, a power transfer occurs between the fundamental mode and the first cladding mode and there is a loss dip in the W-fiber's transmission spectrum. Lastly, in Figure 3.5c, the operating wavelength is much greater than the cutoff wavelength and the fundamental mode has coupled with several of the cladding modes.

This simple mode coupling model can also explain why the loss dips increase as the wavelength increases. As the wavelength increases, the fundamental mode's field spreads further from the core and has more interaction with the cladding modes. Increasing the overlap of the two modes increases the coupling strength, thereby causing more power to be coupled from the core. Eventually the combination of mode coupling and leaky mode loss is so high that power can no longer be transferred from one end of the fiber to the other.

The W-fiber's spectral behavior when the fiber is bent is also explained by the mode coupling picture. Bending an optical fiber introduces a slight birefringence and causes the fiber to have an asymmetrical index profile. The birefringence mostly acts on the outer cladding, therefore there is a slight splitting of the cladding modes. That is, the bending causes one cladding mode to become two cladding modes with slightly different propagation constants. When this splitting occurs, the fundamental mode can couple to the cladding mode at two slightly different wavelengths. This phenomenon was extensively investigated by Steblina *et al* [21].

The mode coupling model is appealing, but does not address certain key issues and there are some complexities involved in using it. None of the mode coupling models directly address what happens to the fundamental mode power once it couples to a cladding mode. In traditional coupled mode theory, the amount of mode power coupled

from one mode to another is periodic with length [8]. If the fundamental mode power is not quickly lost once it couples to a cladding mode, it will completely re-couple back into the core after traveling a certain distance along the fiber. This would mean that the strength of the loss-dips seen in the W-fiber spectrum would be highly length dependent. The mode coupling model also entails some computational complexities. Not only do the propagation constants need to be determined for the fundamental mode, but also for the cladding modes. It is not always certain how to define the regions of the fiber where the cladding modes exist. Lastly, coupling coefficients, which determine the "strength" of the mode coupling, need to be calculated in the mode coupling model. Calculation of these coefficients can be very tedious. The next model for the W-fiber avoids many of the complexities by simplifying how modes are defined and giving the coupling coefficients directly.

3.5.2 Supermode Model

A second model that explains a W-fiber's spectral characteristics is referred to as the "supermode model". In this model, the fiber modes are defined as modes of the entire fiber cross-section (core, claddings, coating, air). These supermodes interact with each other at discrete wavelengths and cause the loss peaks observed in experiments.

In comparison to mode coupling, supermodes are not a concept widely discussed in literature. Hence, this sub-section explains the basics of supermodes. A distinction is made between how modes are perceived in the bound/radiation model (infinite cladding) and the supermode model (finite cladding). The section then shows how supermodes are used to explain W-fiber characteristics. The next section expands on the supermode model by presenting clear experimental evidence that supports the model.

Chapter 2 described how to perform the scalar wave analysis of optical fibers. Boundary conditions within the fiber are used to find the effective index of different modes of the fiber and it was assumed that the fiber's outer layer extended to infinity. This assumption was justified because it was assumed that the field of the fiber's fundamental mode did not penetrate a significant depth into the outer cladding. However, in the case of the W-fiber it has been demonstrated that the width of the outer cladding affects its spectral characteristics. This would suggest that the usual infinite

cladding model may not be entirely accurate for a W-fiber and a new fiber model that takes into account the finite size of the fiber needs to be used.

If a fiber is treated as finite, its boundaries consist of a core, one or more claddings, a protective jacket, and a surrounding medium such as air. Modes calculated based on all these boundary conditions are termed "supermodes" [22].

When a fiber is excited optically, most of the power is launched into the bound, fundamental mode. However, several other fiber modes can be excited. In the case of "normal" fiber analysis, when the cladding is assumed to be infinite, the power not found in the fundamental mode enters into the radiation field. The radiation field can be described exactly in terms of a continuum superposition of radiation modes or approximately in terms of a finite superposition of discrete leaky modes [8]. Since the cladding is assumed to be unbounded, the power entering this radiation field diverges away from the core into the infinite medium as you move longitudinally along the fiber.

In comparison to the bound-radiation mode analysis, in a supermode system, the optical source excites modes of the entire core-cladding-jacket-air profile. Figure 3.6 shows the levels of the effective indices of all the different supermodes superimposed on a simple finite core-cladding-jacket-air refractive index profile. From this figure, it is apparent that the finite fiber system is highly multi-moded.

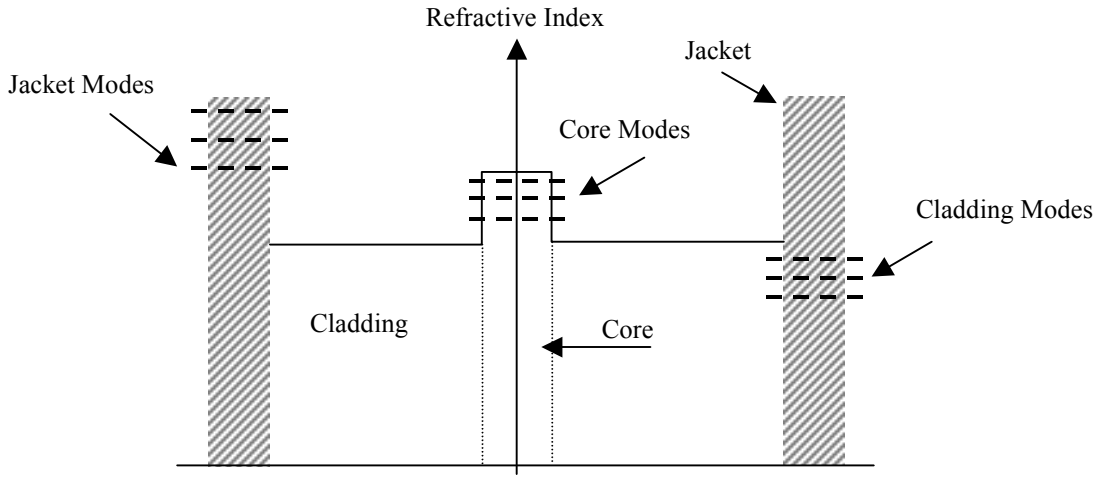

Figure 3.6: Effective index levels of different supermodes.

Since air, which has a refractive index much lower than the indices of the fiber glass or the protective jacket, is included in this model, all of the modes are bound. However, the jacket is very lossy and the "jacket modes" (modes whose fields lie predominately in fiber's jacket) experience a large amount of absorption and scattering [22]. This is also the case for many of the "cladding modes" whose fields are spread out far from the core and have a large interaction with the jacket. This is one of the distinctions between the traditional infinite fiber model and the finite fiber model. In the infinite fiber model, modal loss for the "cladding modes" is due to radiation into the unbounded cladding but in the finite fiber model, modal loss is due to absorption and scattering by the fiber jacket [22].

The modal analysis used for supermodes is similar to that used for modes of the unbounded fiber (i.e. modes must be continuous, boundary conditions must be satisfied, etc). One simplifying condition is that it is assumed that there is negligible penetration of the supermode through the jacket into the air so therefore there is zero mode field at the jacket-air interface [22]. This allows the use of the weakly guiding approximation.

The understanding of supermodes allows the development of a comprehensive model that explains W-fiber characteristics. This supermode model is based on the work of Henry, *et al* [17].

When light is injected into a W-fiber, the fundamental supermode is highly excited, but so too are other higher-order axial-symmetric supermodes. If the light injected into the fiber is at a wavelength below cutoff ($\lambda_o < \lambda_c$), the fundamental supermode (the supermode with the largest effective index) propagates with very little loss and the higher order supermodes suffer significant loss because of their interactions with the lossy fiber coating. As the operating wavelength approaches λ_c, the field of the fundamental supermode spreads out further from the core and "sees" more of the fiber. At a wavelength just greater than the cutoff wavelength ($\lambda_o \approx \lambda_c$), the field of fundamental mode and the first higher supermode interact. At this discrete wavelength, the two supermodes spread out across the transverse direction of the fiber. When this occurs, the fields interact with the lossy surface and a portion of the mode power is lost. When the operating wavelength moves past this point ($\lambda_o > \lambda_c$), the fundamental supermode and the higher order supermode effectively exchange places. That is, the

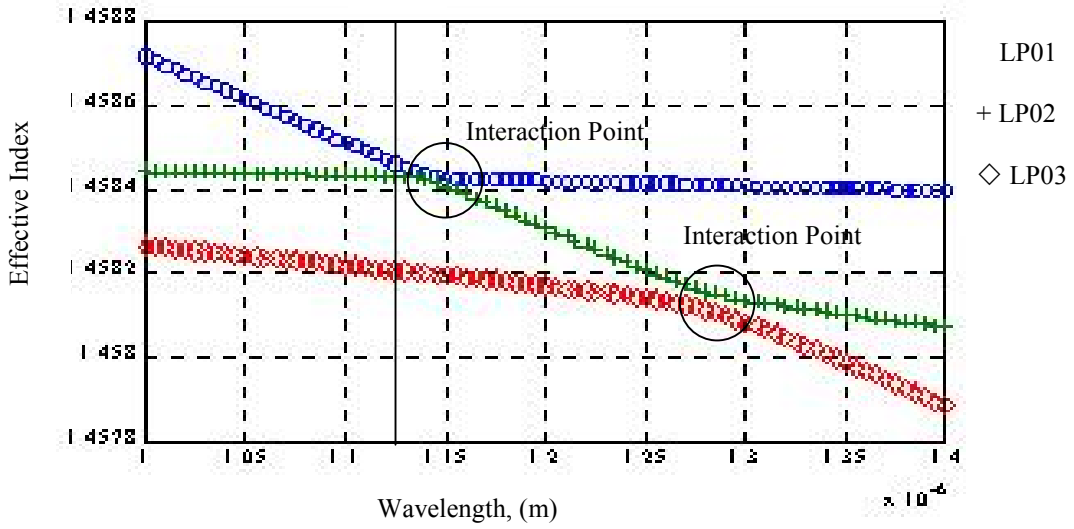

Figure 3.7: Change in effective index over wavelength for the three lowest order supermodes.

mode that was considered to be the fundamental mode now has its field predominately in the outer region of the fiber and the mode that was considered to be the higher order cladding mode now has its field mostly contained within the core. This supermodal interaction at discrete wavelengths continues as the operating wavelength increases. At each interaction point, the amount of power lost increases because the modes are spread out further from the core and have greater interaction with the lossy coating.

Figures 3.7 and 3.8 demonstrate the concept of supermode interaction. In Figure 3.7, the effective indices for the three lowest supermodes are plotted against wavelength. At wavelengths less than λ_c, the fundamental mode (designated LP01) has an effective index that decreases monotonically with increasing wavelength. The effective indices of the LP02 and LP03 modes change very little over this same range of wavelengths. This is because the LP01 mode field is confined mostly to the core and inner cladding of the fiber and "sees" a larger index differential as the wavelength changes. Soon after λ_c, the LP01 and LP02 modes have an interaction point at a discrete wavelength. Here the mode fields undergo a significant change (shown in Figure 3.8). It is at this wavelength that a loss peak appears in the W-fiber's spectrum. Immediately after this wavelength, the LP01 curve continues with the same slope as the LP02 curve and the LP02 curve takes on the same slope as the LP01 curve. In this way, the LP01 and the LP02 modes

"exchange places" [17]. The LP02 effective indices now begin to change rapidly with the increasing wavelength. Eventually another interaction point is reached, this time between the LP02 and LP03 modes. Again, the modes "exchange places".

In Figure 3.8, the field amplitudes of the first two supermodes (LP01 for the fundamental supermode and LP02 for the first higher order supermode) are shown for

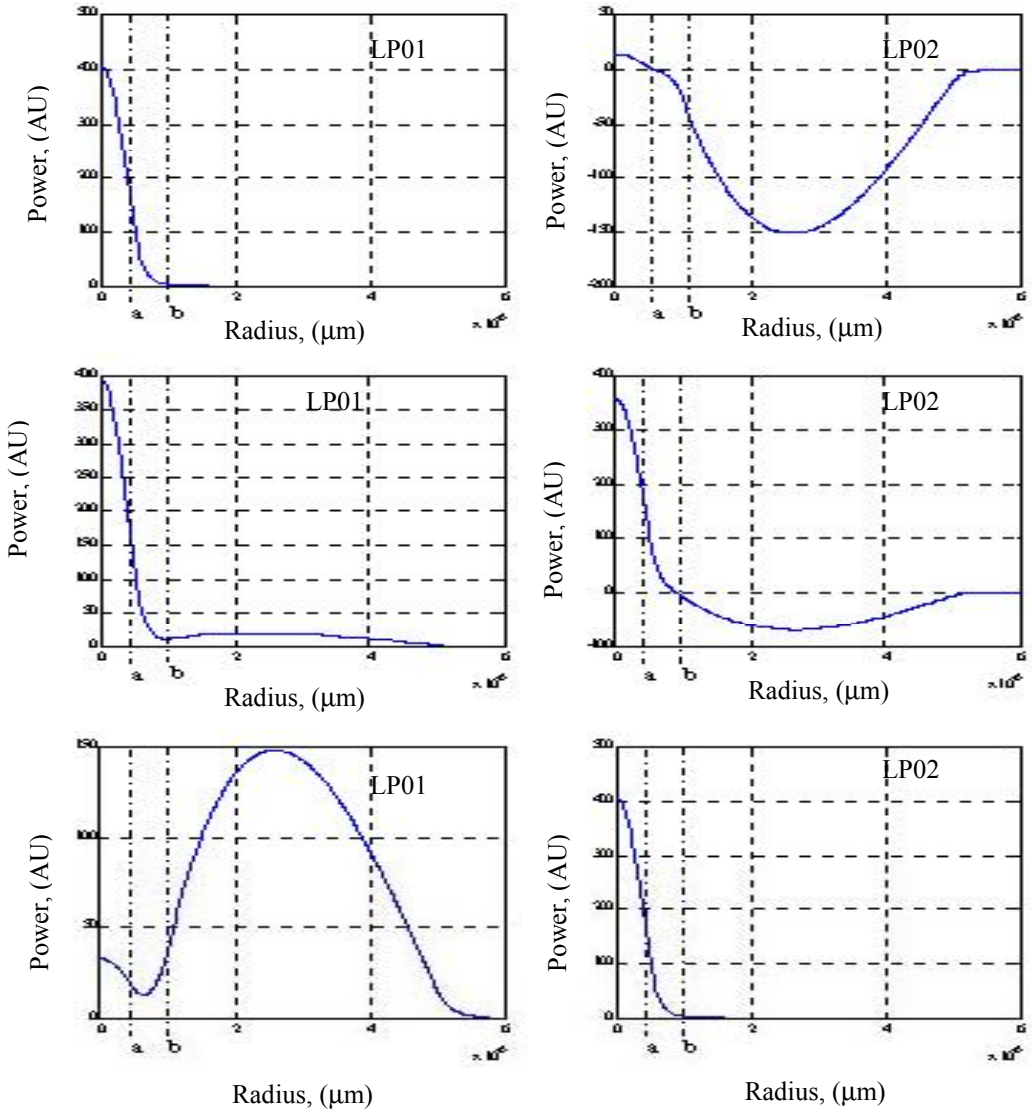

Figure 3.8: Mode fields for the LP01 and LP02 supermodes in a W-fiber. (a.) W-fiber is operating at $\lambda < \lambda_c$. (b.) The operating wavelength is slightly greater than λ_c. (c.) W-fiber is operating at $\lambda > \lambda_c$.

different operating wavelengths. In Figure 3.8a, the operating wavelength is much less than cutoff. The LP01 mode is well confined to the core, spreads slightly into the inner

cladding, and has negligible field strength in the outer cladding. The field of the LP02 mode is spread far into the outer cladding with only some of its field in the core and inner cladding. Just above the cutoff wavelength, shown in Figure 3.8b, the situation is very different. Both modes have a significant portion of their fields spread across the fiber cross-section. This wavelength corresponds to a loss peak on a wavelength scan because the LP01 mode is interacting with the LP02 mode which experiences significant loss due to the fiber coating. In Figure 3.8c, the operating wavelength has moved well past the cutoff wavelength. Now what is considered the fundamental mode has spread out so most of its field lies on the outer cladding. Its field shape now resembles the field shape of the LP02 mode. The LP02 mode is now well confined to the fiber core. This graph corresponds to the area on the plot in Figure 3.7 where the first two modes have "exchanged places".

The next section presents experimental evidence that directly supports this supermode model. It also gives results of a computer simulation written based on the supermode model and compares the simulated with the experimental results.

3.6 Experimental and Simulation Data in Support of Supermode Model

This section is divided into two subsections. The first subsection presents data from experiments performed to specifically test the supermode model of W-fiber spectral characteristics. This subsection describes the experimental setups and interprets the important results of the experiments. The second subsection presents results from a computer simulation in which a W-fiber is modeled based on the supermode picture. It is shown that the experimental data and simulation results are in good agreement with each other and the supermode model is an easy and effective way to model W-fibers.

3.6.2 Experimental Results

The W-fiber used in all of the experiments is a test fiber produced at Bell Laboratories. Several meters of fiber with varying diameters were drawn from the same preform. The sizes of the W-fiber samples were in the range of 100 – 150 μm for their outer diameter and 5 – 9 μm for their core diameter.

The first experiment helped determine what happened to the mode power once it leaves the core of the W-fiber. The experiment compared the W-fiber spectrum when only the core light is collected to the W-fiber spectrum when light from the entire cross-section is collected. The experiment involved two steps. First, the spectrum of a 0.75 m sample of W-fiber was measured. Light was injected and collected from the W-fiber using SM fibers. As expected, the measured spectrum showed the usual discrete loss peaks. Next, the output SM fiber was replaced with a piece of Corning PowerCore fiber with a 200 μm diameter core to collect the light from the entire cross-section of the W-fiber. Figure 3.9 is the schematic of the experimental setup with the Corning multimode (MM) fiber at the output. The configuration in Figure 3.9 ensured that the W-fiber could be held straight and therefore the loss peaks would not be distorted by curvature in the W-fiber. Since the total diameter of the test W-fiber was only approximately 100 μm, it was certain that the MM fiber collected light from the entire W-fiber cross-section. The W-fiber spectrum measured when the MM fiber was used for the output matched exactly with the spectrum measured when only a SM fiber was used for the output. This shows that the light removed from the core of the W-fiber does not propagate a significant longitudinal distance in the cladding and this indicates there must be some sort of mechanism in place to cause the light to be permanently lost.

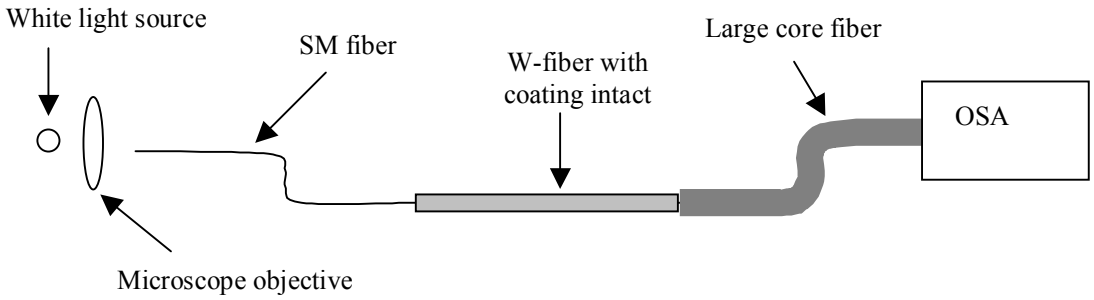

Figure 3.9: Experimental setup for measuring light collected from entire W-fiber cross-section.

The idea that the core light is lost permanently is supported by a series of cutback experiments. In these experiments, different samples of W-fiber were cut back 1 – 2 cm at a time and the fiber spectrum was measured after each cut. Typically, the W-fibers

were cutback from approximately 40 cm to around 10 cm. Cutting the W-fiber shorter than 10 cm became unreliable since the fiber tended to break, the cleave quality was less consistent, and the amount of fiber cutback was difficult to control. If the loss peaks seen in the W-fiber spectrum were due to mode coupling between the fundamental mode and discrete cladding modes and the coupled light was guided in the cladding, one would expect to see a characteristic beat length at the wavelengths where a loss peak occurred. Based on coupled mode theory, this characteristic beat length would be wavelength dependent. The cutback experiments did not reveal any sort of beat length. The change in loss only appeared to be length dependent.

Since now it is clear that the light lost from the core is lost permanently, the next step is to clearly establish the role of the fiber coating in the W-fiber's spectrum. Two experiments in which samples of W-fiber were suspended vertically helped determine this. Figure 3.10 shows the general setup of the vertical experiments. In these

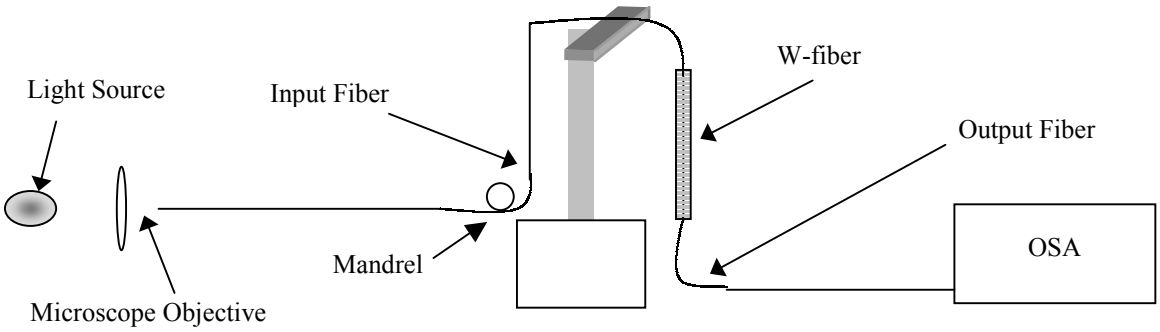

Figure 3.10: Experimental setup for vertical W-fiber measurements.

experiments, a SM fiber was used to inject light into a sample of W-fiber. The SM fiber used for the input had a smaller core than the W-fiber (7.2 μm diameter versus a 9 μm diameter respectively) and was specified to be single-moded at approximately 700 nm. This ensured that the modal excitation was on axis to the W-fiber and light was not inadvertently launched into the cladding. The input fiber was also wrapped twice around a 2 cm diameter mandrel to suppress any higher order modes that may have been inadvertently excited. The W-fiber was suspended vertically so it was not in contact with any other surface and was short enough so that it could be pulled taught thus ensuring no

bends in the fiber. The output of the W-fiber was collected using either a SM or MM fiber and measured on an OSA.

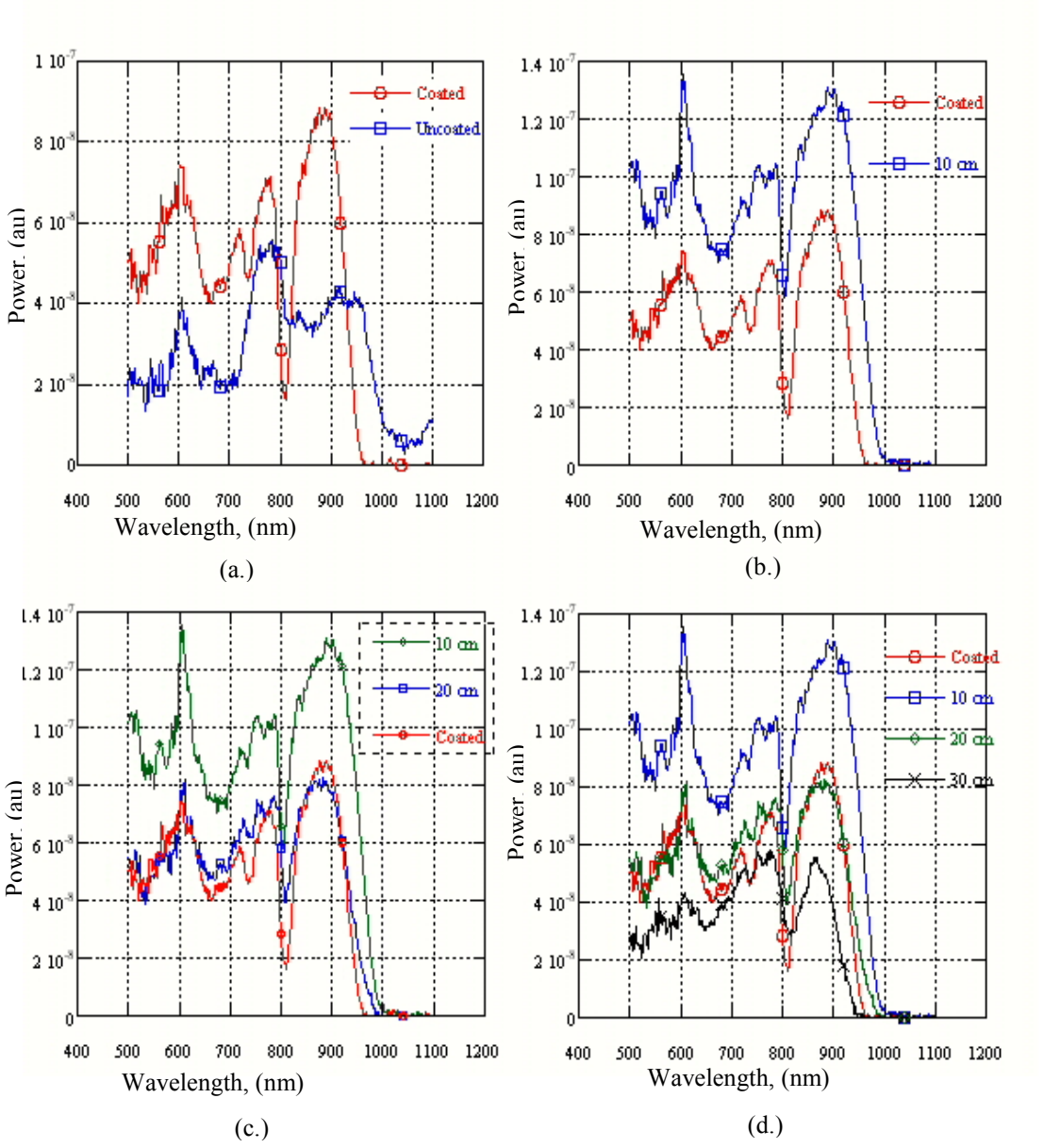

Figure 3.11: Results from first set of vertical measurements. (a.) Original W-fiber spectrum and spectrum from the entire cross-section of an uncoated W-fiber. (b.) – (d) W-fiber spectrum with successive amounts of coupling gel.

In the first vertical experiment, Corning PowerCore fiber was used as the output fiber and the W-fiber was approximately 40 cm long. Five different measurements of the W-fiber were taken. In the first measurement, the coating of the W-fiber was left intact.

Again, the spectral response of the W-fiber showed the expected discrete loss peaks and a complete extinction of mode power after a certain wavelength. For the second measurement, the coating of the W-fiber was completely removed and the measured response was very different. The loss peaks were washed out and power was measured at wavelengths where previously there was zero throughput in the system. The spectra of the coated and uncoated W-fiber are shown in Figure 3.11a. Since the PowerCore was collecting the light from the entire cross-section of the W-fiber, this indicates that the light lost from the core was located in the cladding and could propagate in the absence of the highly lossy coating. This agrees well with intuition. Since the uncoated fiber is surrounded by air, which has a refractive index close to unity, the cladding itself can act as a waveguide when it is surrounded by materials of a lower refractive index. The use of a small core single mode fiber as the input to the W-fiber makes it unlikely that light was launched into the cladding of the W-fiber and therefore light found in the cladding came from light originally in the core. The structure seen in the uncoated spectrum is due to the spectral response of the light sources, input and output fibers and the OSA photodetector. The next three measurements taken with the vertical setup were done with varying amounts of high-index coupling gel on the W-fiber. Gel was placed on a 10 cm, 20 cm, and 30 cm of the W-fiber. The progression of how the spectrum of the recoated W-fiber changed is shown in Figures 3.11 b - d. The gel clearly caused the W-fiber spectrum to revert to its original response. This experiment indicates that how the surface of the W-fiber is treated greatly affects the fiber's spectral response.

The second vertical experiment was very similar to the first vertical experiment except that a SM fiber was used for the output fiber. Using a SM fiber at the output ensured that only light from the core was collected. Again, the response of the W-fiber was measured under several different conditions. First, the response of the W-fiber with its coating intact was measured. This response is shown in Figure 3.12a. Next, the coating of the W-fiber was completely removed and the response was re-measured. This response is shown in Figure 3.12a superimposed on the original W-fiber response. The same discrete loss peaks at lower wavelengths are still there, but now there is power measured at wavelengths well beyond where there was no signal before. In addition, this extra signal shows the same sort of discrete loss peaks seen at

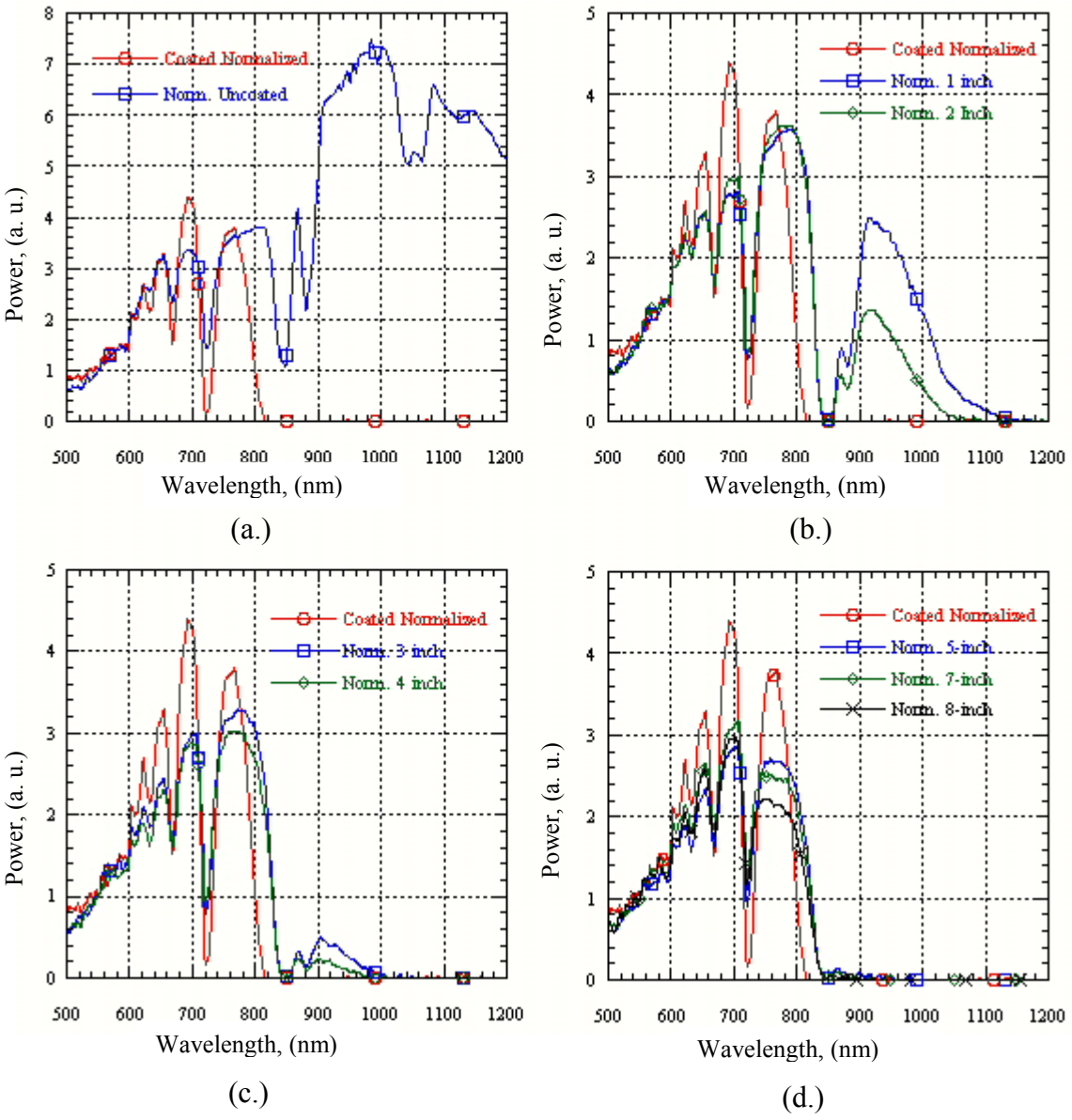

Figure 3.12: Results from second vertical W-fiber experiment. (a.) Spectral response from the jacketed W-fiber and the response from the unjacketed W-fiber. (b.) – (d.) Changes in the response as coupling gel is applied to the bare fiber.

the lower wavelengths. This would indicate that in the absence of a highly lossy interface at the fiber's outermost boundary, the light removed from the fundamental mode in the core remains within the fiber and is available for a seemingly endless number of modal interactions. The plots in Figures 3.12b – 3.12d show the effect of applying coupling gel to the uncoated W-fiber in sections 2.5 cm long. It is immediately apparent that by applying the gel to the bare fiber, even in small quantities, the extraneous signal seen at

the longer wavelengths is well suppressed. Applying gel in sections longer than 10 cm (Figure 3.12 d) does not seem to have much effect on the spectrum. This is in good agreement with what was observed in the cutback experiments. The signal seen with the uncoated fiber suggests that if there is not a lossy interface on the fiber's surface, the mode power that is removed from the core remains within the fiber to beat in and out of the core. In the cutback experiments, spectra for W-fibers shorter than 10 cm were usually unobtainable and no beat length could be found in the longer sections of W-fiber. In both cases 10 cm of a highly lossy interface on the fiber's surface is enough to ensure that the power removed from the core is completely scattered and lost.

The results of experiments summarized in this subsection help legitimize the supermode model of W-fibers. The next step in validating this model is the development of a simulation based on the supermodes picture.

3.6.2 Results of Computer Simulation

This section summarizes the results of a computer simulation based on the supermode model of W-fibers. The simulation calculates the propagation constants of the lowest order supermodes and, based on these values determines at which wavelengths the loss peaks in the W-fiber spectrum are found.

The simulation uses a relatively simple algorithm. Values are assigned to the parameters shown in the general fiber model in Figure 3.13. The terminology for the

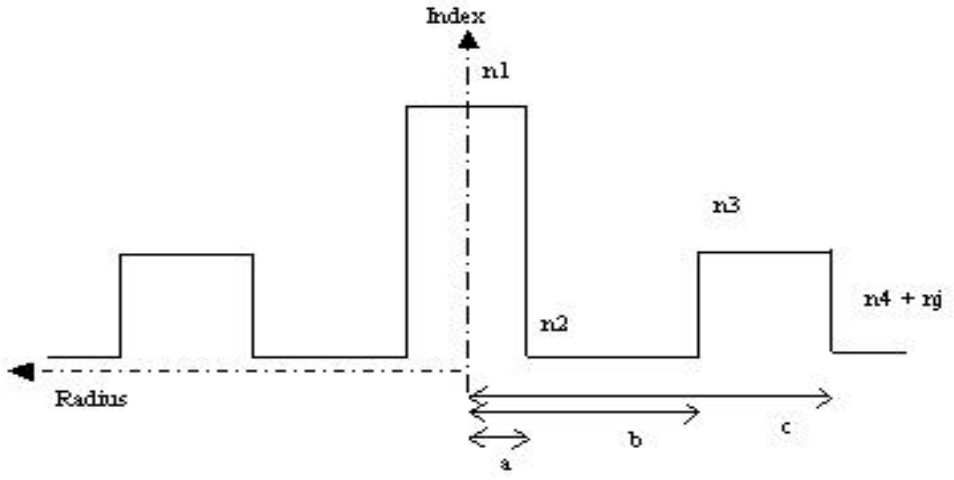

Figure 3.13: Index profile used in W-fiber computer simulation.

fiber parameters is the same as those used in Figure 3.1. The values for the core and inner cladding radii and the values for the refractive indices ensure that the weakly guiding approximation is valid and that there will be a cutoff wavelength for the fundamental mode. It is important to note that the simulation adds a fourth layer to the fiber. This means that the width of the outer cladding can be used as a variable and the effect of its width on the W-fiber's spectrum can be determined. The fourth layer (which represents the fiber's coating) is shown to have a lower index than the outer cladding. In reality, this is not the case, but it helps avoid numerical problems when running the simulation. In addition, as is shown shortly, the loss caused by the coating can be approximated by adding a small imaginary number, n_j, to its real index value, n_4[17].

The simulation defines the mode field in the core and inner cladding the same as in section 3.2. However, now the field in the outer cladding must be defined in terms of the I and K Bessel functions for neff > n_3 and in terms of the J and Y Bessel functions for neff < n_3. The field in the outermost region (the coating) is still defined in terms of the K Bessel function.

With the mode field defined and the fiber parameters set, the simulation searches for a non-trivial solution to the fiber's eigenvalue equation over a range of wavelengths. The first solution corresponds to the lowest order supermode, the next solution is the next highest supermode and so on. Solutions to the eigenvalue equation are used to find the value of the propagation constants and hence the value of the modes' effective indices at different wavelengths.

Calculations for the simulated W-fiber spectrum are based on the fiber's excitation conditions and a small loss perturbation added to the fiber's jacket. For simplicity, it is assumed that the input to the fiber is Gaussian beam [17]. The amplitude coefficient is determined by an overlap integral defined as:

$$A_i = \frac{\int_0^\infty \psi_i \exp\left\{-\frac{1}{2}\left(\frac{R}{a}\right)^2\right\} RdR}{\int_0^\infty \psi_i^2 RdR} \qquad 3.10$$

where A_i is the amplitude coefficient, ψ_i is the mode field, and a is the core radius. The total power transmitted by the supermodes over a length of W-fiber is given by:

$$P_t = A^2_i \exp(-2\beta_{im} z) + A^2_{i'} \exp(-2\beta_{im'} z) + \ldots \quad 3.11$$

where z is the distance along the fiber and β_{in} is the imaginary part of the modal propagation constant due to the field's interaction with the fiber jacket. β_{im} is defined as:

$$\beta_{im} = k n_j \eta \quad 3.12$$

where k is the wavenumber, n_j is the real value of the small imaginary perturbation and η is the fraction of the mode power in the fiber jacket. The value of n_j is somewhat arbitrary. The larger its value, the stronger the loss caused by the fiber coating.

First, the simulation was validated by comparing calculated values from a "supermode" W-fiber to values from a "normal" W-fiber (i.e. a W-fiber defined with only 3 layers and it is assumed the outer cladding extends to infinity). As can be seen in Figure 3.15, the solutions for both fiber models are in good agreement with each other. The plot shows the values of the effective index of the fundamental mode for both fiber models over a range of wavelengths. The close agreement in values shows that when the W-fiber is operated at wavelengths less than the cutoff wavelength, the infinite cladding model is accurate. Other works support this same conclusion [16] [20].

Another validation of the supermode simulation is a calculation of how varying the W-fiber's parameters effects the cutoff wavelength. Figure 3.16 shows the change in the normalized cutoff frequency for different ratios of b/a. The normalized cutoff frequency has the same definition as the normalized frequency in equation 3.5 except λ_c is substituted for λ. Each curve in the plot corresponds to a different value of $\Delta n'/\Delta n$. As expected, as the value of $\Delta n'/\Delta n$ increases, the cutoff wavelength increases. This is because the larger $\Delta n'/\Delta n$ is, the less deep the inner cladding is relative to the outer cladding and therefore the less effect it has on the effective index of the fundamental

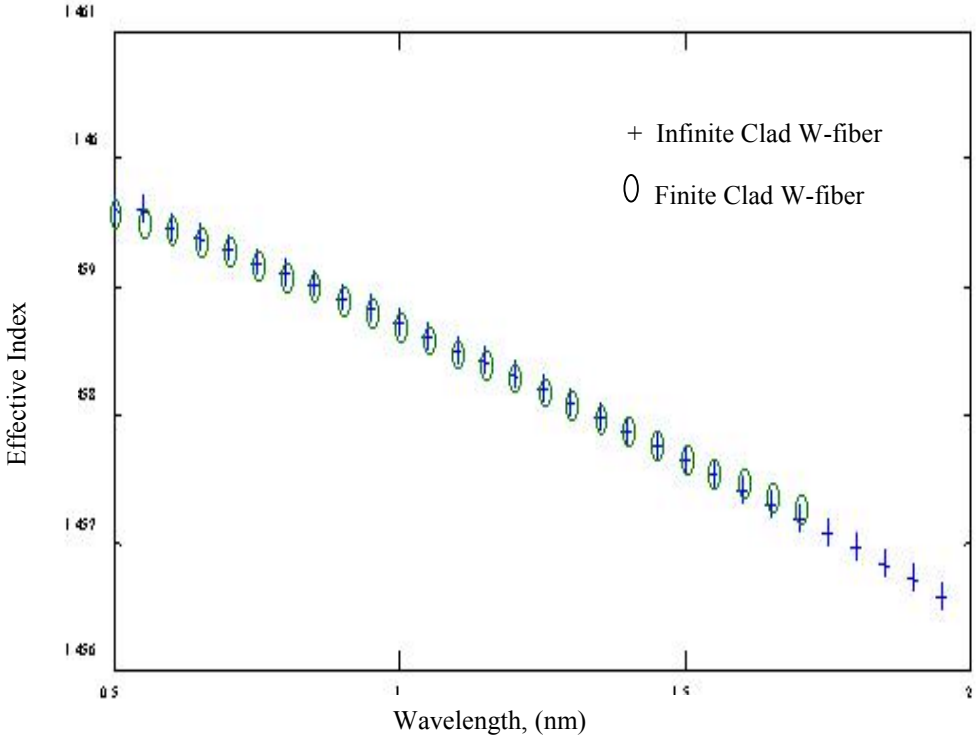

Figure 3.14: Comparison of the effective indices of the fundamental mode in a W-fiber for $\lambda < \lambda_c$.

mode. Increasing the ratio of b/a after a certain point does not appreciably affect value of the cutoff wavelength. This is because at wavelengths less than cutoff, the fundamental mode field decays rapidly outside of the core and therefore only "sees" part of the inner

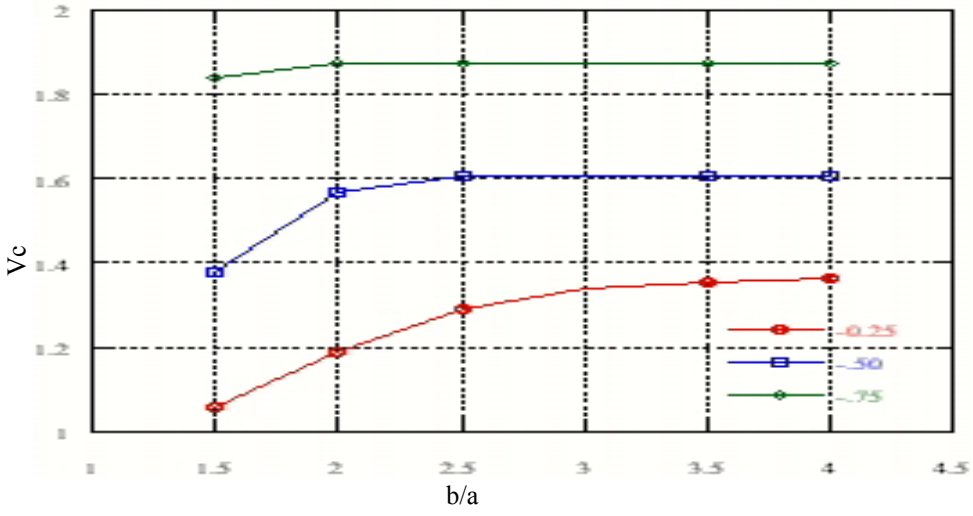

Figure 3.15: Change in Vc for increasing b/a. Each curve represents a different ratio of $\Delta n'/\Delta n$.

cladding. Therefore expanding the inner cladding past a certain size does not have much effect on the fundamental mode's effective index.

The next step is to use the simulation to understand how varying the W-fiber design parameters affects the interaction of the different supermodes and how this interaction affects the fiber's spectral characteristics.

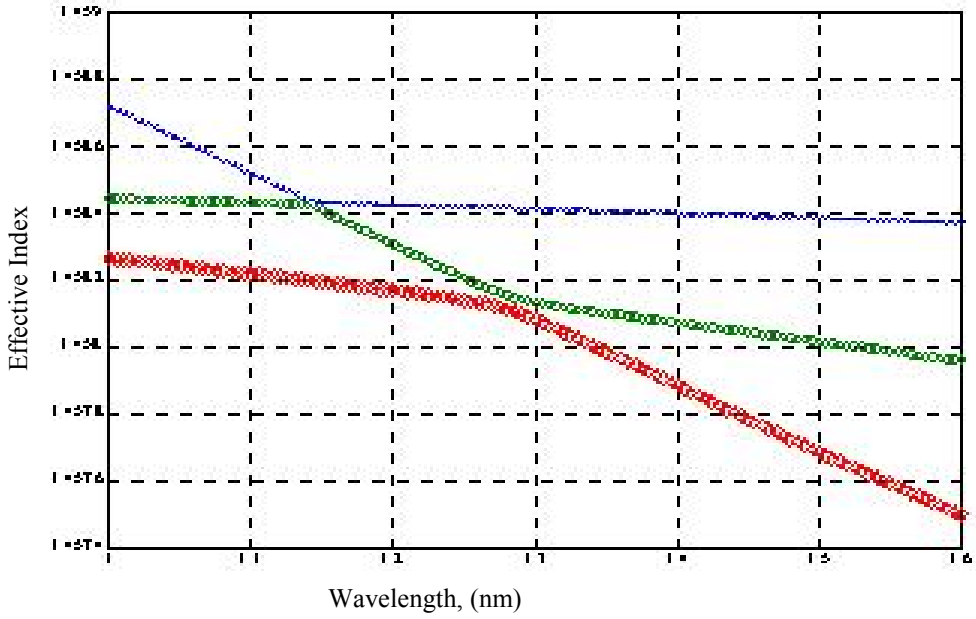

Figure 3.16a: Plot of neff vs. λ for the three lowest supermodes.

A preliminary simulation establishes that the anomalous loss peaks seen in the W-fiber spectrum occur at wavelengths where the supermodes interact with each other. Figure 3.16a shows the effective indices over a range of wavelengths for the three lowest supermodes (designated LP01, LP02 and LP03) in a W-fiber designed so that b/a = 2, $\Delta n'/\Delta n = -0.75$, and c = 45 μm. The coating was given a small loss factor of $n_j = 1 \times 10^{-4}$. The cutoff wavelength for this system is approximately 1.12 μm. The points in the curves where the value of the modal effective index undergoes a sharp change are the wavelengths at which the supermodes interact. The first supermodal interaction occurs soon after λ_c at 1.14 μm and the second interaction occurs at 1.28 μm. Even though the curves are very close together at these wavelengths, they do not actually touch. Figure 3.16b is the simulated spectrum for the above parameters. The loss peaks seen in the

spectrum are at the same wavelengths where the supermodes interact on the effective index plots.

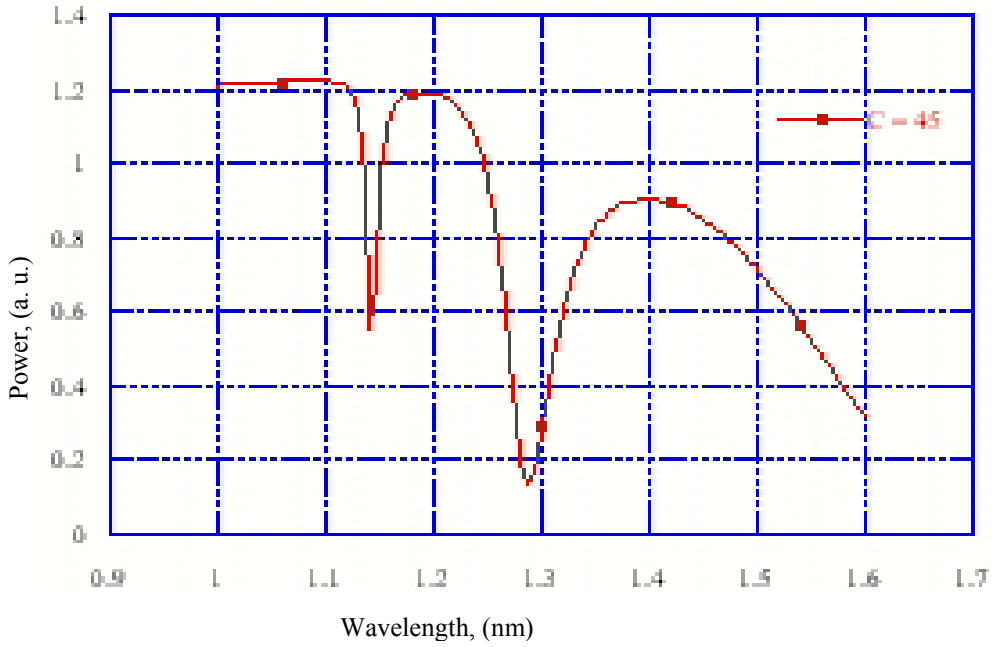

Figure 3.16b: Spectral response of W-fiber with c = 45 μm.

The first set of simulations considers what happens when the width of the outer cladding is varied. The results of these simulations should agree with the observations made in the index matching experiment. That is, as the W-fiber's outer cladding approaches infinity, the loss peaks should wash out and the fiber's spectral response should have a step loss. Figure 3.17 shows how the spectral response of a W-fiber with the parameters b/a = 2, $\Delta n'/\Delta n = -0.75$, and $n_i = 1x10^{-4}$ changes as its outer cladding width is varied from c = 40 μm to c = 60 μm. Several facts are apparent from these plots. First is the shift in the loss peaks as the cladding width changes. The fibers with the smallest outer cladding have loss peaks occurring at the longest wavelengths. As the cladding size increases, the dips get weaker and shift to lower wavelengths. The weaker dips are due to the fact that with a large outer cladding, there is less mode field interaction with the lossy jacket. The shift to shorter wavelengths are due to the rate of change with wavelength of the effective indices of the LP02 and LP03 supermodes. With a large cladding, the fields of these modes are mostly contained to this region of the fiber and do not "see" as much of the lower index inner cladding. Therefore, as the

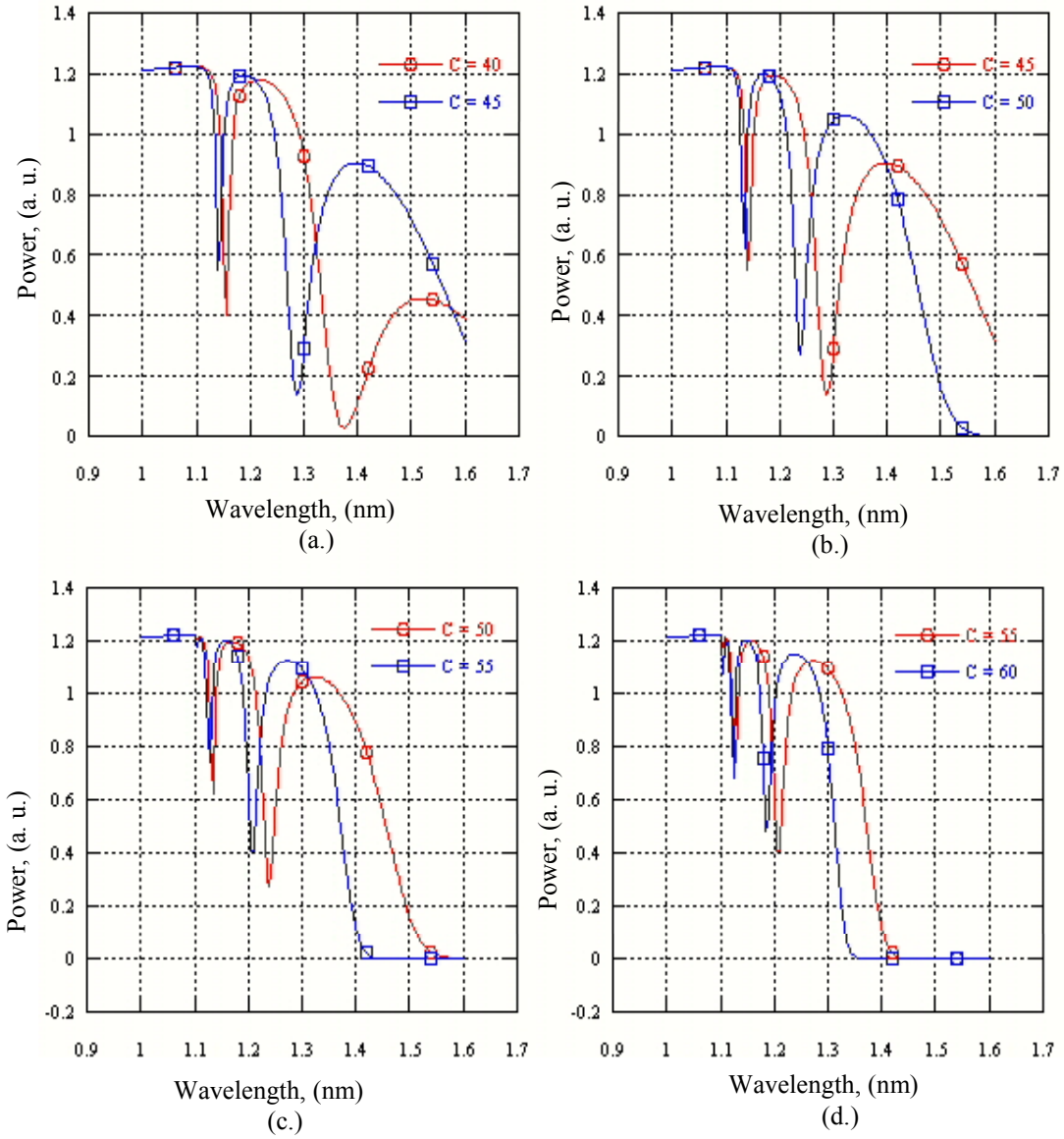

Figure 3.17: Changes in the W-fiber's spectral response due to changes in the width of the outer cladding.

wavelength increases, their effective indices do not decrease very much and they can interact with the LP01 supermode at a shorter wavelength. Figure 3.18 compares the effective indices of the LP02 mode for W-fibers with outer cladding thicknesses of 45 μm and 60 μm. The rate of change of the effective index of the LP02 mode for the 45μm fiber is much more than for the 60 μm fiber. Another observation from the curves is that for fibers with a relatively small outer cladding, even at wavelengths where there is not a significant interaction of the supermodes, the fundamental mode experiences a noticeable

loss. This is due to the fact that at wavelengths longer than cutoff, even though a higher order supermode is concentrated in the core after an interaction wavelength (see Figure 3.12), it is not as well confined as the fundamental mode is at wavelengths less than cutoff. Therefore, in a fiber with a relatively thin outer cladding, the less well confined mode has a slight interaction with the lossy coating.

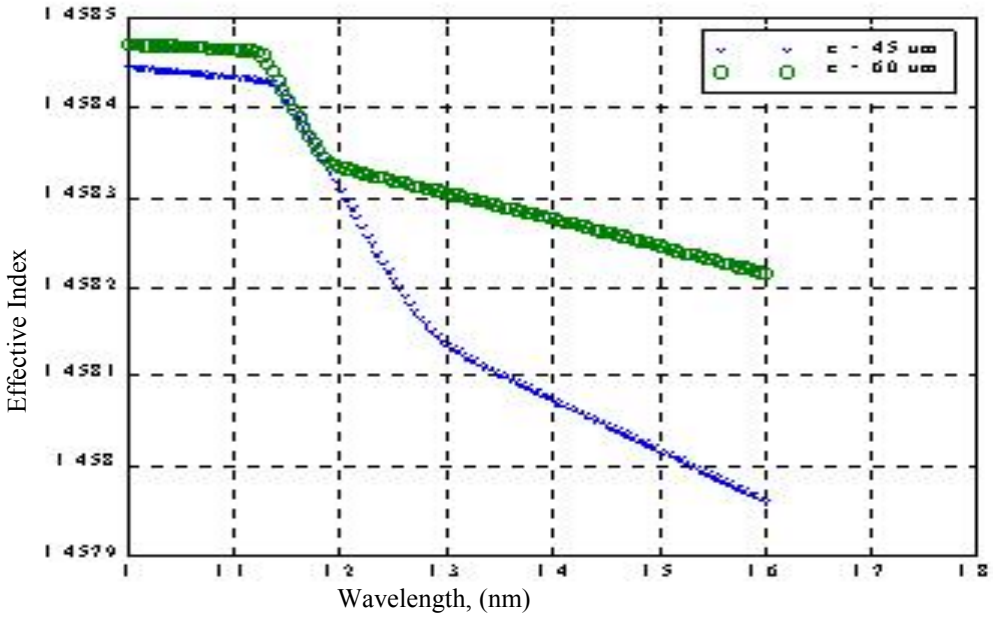

Figure 3.18: Change in slope of the LP02 neff curves for different cladding thicknesses.

A second set of simulations compares the effects of different values of b/a on W-fiber characters at wavelengths greater than cutoff. Figure 3.19 shows the output spectrum for three W-fibers b/a ratio values of 1.5, 2, and 2.5. It is apparent that changing b/a ratio does not have a large effect on the relative position of the interaction wavelengths. This is in good agreement with the b/a versus Vc plot in Figure 3.12, where once the ratio of b/a exceeded a certain value, there was very little change in the wavelength at which Vc occurred. One area where the value of b/a has a large effect is the loss experienced at the interaction wavelengths. As can be seen in Figure 3.20, as b/a increases, the loss peaks become weaker. Again, this is because the thicker the inner cladding becomes, the less interaction the supermodes will have with the fiber's coating.

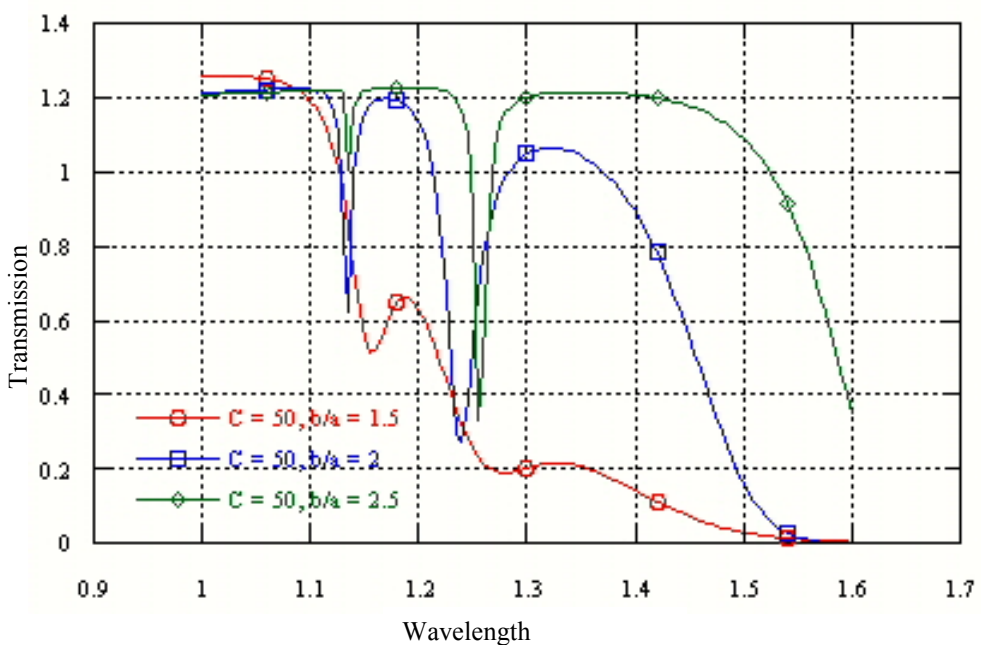

Figure 3.19:Change in W-fiber output spectrum for different ratios of b/a.

The data from the computer simulation based on the supermode model of W-fibers agrees well with published results and experimental data. Therefore it appears that the supermode model is a good model to use when considering what happens in a W-fiber when it is operated at wavelengths longer than cutoff.

3.7 Applications of W-fibers

An optical fiber with a depressed cladding obviously gives the fiber special spectral properties that are not possible in a matched cladding fiber. The high sensitivity to bending makes the W-fiber useful in fiber optic sensor systems. The existence of an "extinguish" wavelength allows the W-fiber to be used for a low pass filter. Published results describe the use of W-fibers as all fiber filters [23]. However, as was shown in the previous section, the W-fiber spectrum not only contains a point at which no power can be transferred from one end of the fiber to the other, but there are multiple weaker loss peaks. Therefore, care must be taken as to which wavelength range the W-fiber is used so those smaller loss peaks do not interfere with the system's overall performance. In addition, if the loss peaks are utilized for some special application, it is important to

understand which loss peak is being used and where the others are located. (This point is addressed in a later chapter).

As has already been demonstrated, the parameters of the W-fiber will determine its spectral performance. Therefore, W-fibers with two different refractive index profiles and/or physical dimensions can have different cutoff wavelengths. The next section discusses how this fact is used to construct a special type of all fiber device: the single polarization fiber.

Chapter 4:

Single Polarization Optical Fibers

This chapter focuses on a specific application of depressed cladding fibers: the fiber polarizer. A highly birefringent fiber with a depressed inner cladding is able to polarize the light launched into it. These fibers can be thought of as an all-fiber alternative to bulk polarizers.

This chapter is divided into four sections. The first section reviews the structure of the single-polarization fiber. It also describes how this type of fiber polarizer is designed and why it is different from other fiber polarizers that are available. The second section describes how the polarizer works. The third section presents some of the examples of spectral responses measured from the fiber polarizers. The last section summarizes some the problems encountered when using these devices.

4.1 Overview of Single Polarization Fibers

This first section describes the structure of the W-type single polarization fiber, compares it to other fiber polarizers and briefly lists some fiber polarizer applications. The next section lists details of how the polarizer operates and why it has the characteristics that it does.

As shown in Figure 4.1, the W-type fiber polarizer is composed of several layers – core, inner cladding(s) and outer cladding. The secondary cladding is an optional component, which will be discussed in the next section. The W-type polarizer is highly elliptical, having almost a slab waveguide structure along its longest dimension. This ellipticity is achieved using a special preform deformation technique [24]. In this technique, after the preform is collapsed, it is heated to the point of softening and compressed from the side with large slabs. As the preform is drawn into a fiber, the draw temperature and speed are controlled to assure that the fiber remains elliptical.

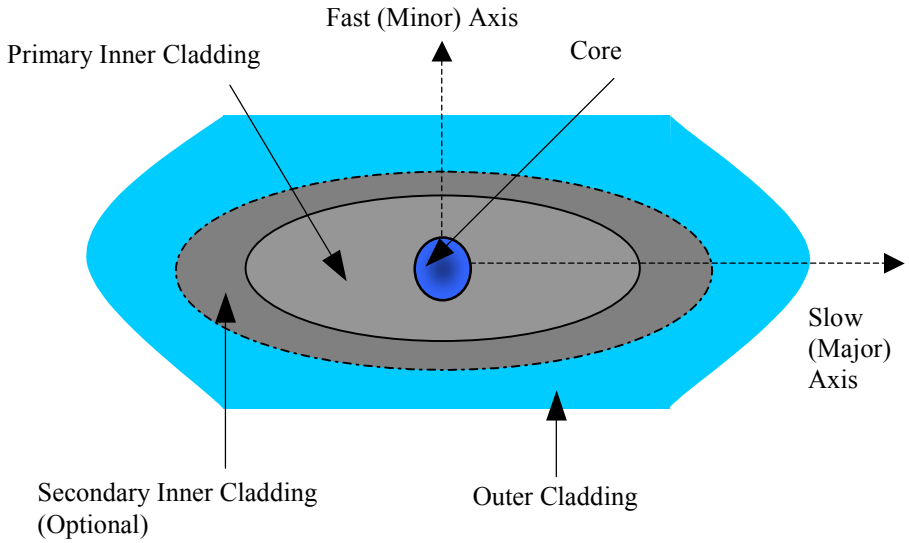

Figure 4.1: Cross-section of a W-type fiber polarizer.

Single polarization fibers remove the mode power from one of the fiber's eigenaxes. Therefore, the output of a single polarization fiber is a mode that is truly linearly polarized. (Even though an LP approximation is used in the weakly guiding assumption, modes of a standard fiber are only approximately linearly polarized.) A distinction should be made between single polarization fibers and polarization maintaining (PM) fibers. PM fibers are also highly birefringent but they do not induce loss in one of the axes of polarization. Instead, these fibers guide the fundamental mode over a long distance without causing a change in the mode's state of polarization.

Single polarization in fibers can be made using several different techniques including various internal and external methods. An example where the polarizing is achieved through an internal mechanism is to create a fiber with stress lobes on either side of the core [25]. Examples of polarizing using external mechanisms include side polishing the fiber and using fused taper couplers [26] [27].

4.2 Principals of Polarizer Operation

Understanding the properties of a depressed cladding fiber help in the understanding of how the W-type fiber polarizer polarizes light. This section examines how the W-type polarizer operates by connecting it with the properties of depressed

cladding fibers. To begin with, this section reviews the concept of polarization in fibers. Next, some details regarding birefringence in fibers is examined. Finally, the idea of differential loss as a mechanism for achieving single polarization is described.

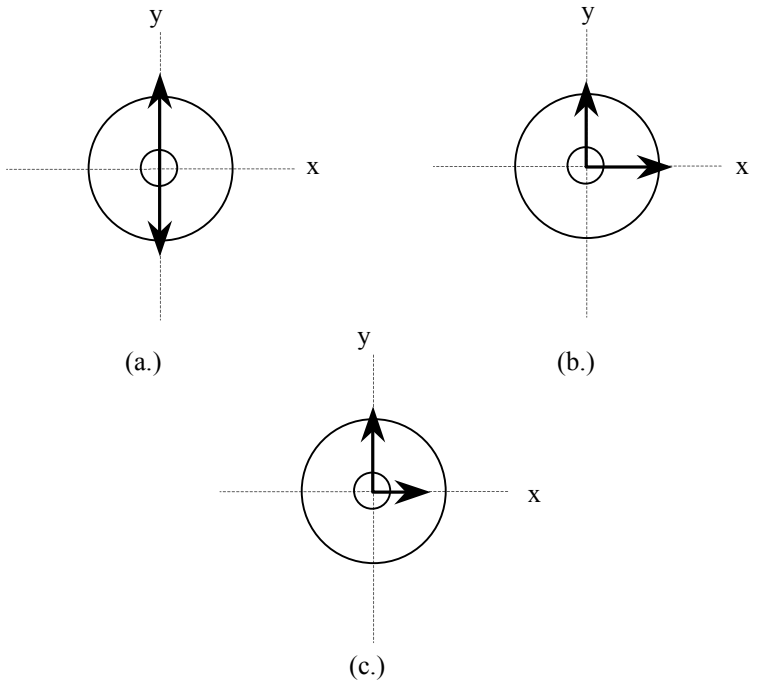

Figure 4.2: Schematic of the states of polarization in an optical fiber. (a.) Linear polarization (b.) Circular polarization (c.) Elliptical polarization

Light launched into a SM fiber has a random state of polarization. The state of polarization (either linear, elliptical, or circular), is determined by the amount of energy from the light pulse that is decomposed onto the fiber's eigenaxes. Figure 4.2 is a schematic of this concept. In the figure, the x and y axes are the fiber's eigenaxes. In a perfect fiber, which has arbitrary eigenaxes, light launched with a particular state of polarization will remain in this state. However, no fiber can ever be perfect. Random imperfections are created when the fiber is drawn and further imperfections are introduced when the fiber is cabled and deployed. The imperfections are distributed randomly along the length of the fiber and therefore the state of polarization of the pulse can change in a random fashion along the fiber. These imperfections along the length of the fiber will cause light along one eigenaxis to be coupled to the other eigeneaxis. From

examining Figure 4.2, it can be seen that if some of the power along the x-axis in Figure 4.2a is transferred to the y-axis, the light will become elliptically polarized as in Figure 4.2 c.

This random change in polarization state is not a serious concern in most fiber optic systems. Most communication systems are based on on-off keying (OOK) where the intensity of the pulse received determines if a "1" or a "0" was sent. The photodetector is a square-law device that has a low polarization dependence.

The ellipticity of the fiber causes a high birefringence within the fiber. Birefringence is the difference in the effective indices of the modes that are aligned along the eigenaxes [28]. Therefore, birefringence is defined as [28]:

$$B = n_x - n_y = k(\beta_x - \beta_y) \tag{4.1}$$

In equation 4.1, B is the overall birefringence of the fiber, n_x is the effective index of the mode power along the x-eigenaxis, and n_y is the effective index of the mode power along the y-eigenaxis. In Chapter 2, it was shown that the modal effective index is partially determined by the refractive index of the fiber. Therefore, birefringence causes a slight change in the refractive index of the fiber. Birefringence can be induced externally or internally. In the case of the W-type fiber polarizers, the birefringence is due to both the external shape of the fiber and the shape of the internal regions of the fiber. The result of the high birefringence is to cause each axis to have a distinctly different refractive index profile. Figures 4.3a and 4.3b schematically show the index profiles of the major and minor axes of the W-type polarizer superimposed on each other. Figure 4.3a is the structure of the three-layer polarizer and Figure 4.3b is the structure of the four-layer polarizer. For the remainder of this thesis, polarizers with only one inner cladding are referred to as three-layer polarizers and polarizers with two inner claddings are referred to as four-layer polarizers. From these diagrams, it can be seen that the birefringence is localized to the core and inner cladding regions of the fibers and the outer cladding has the same index value along each axis.

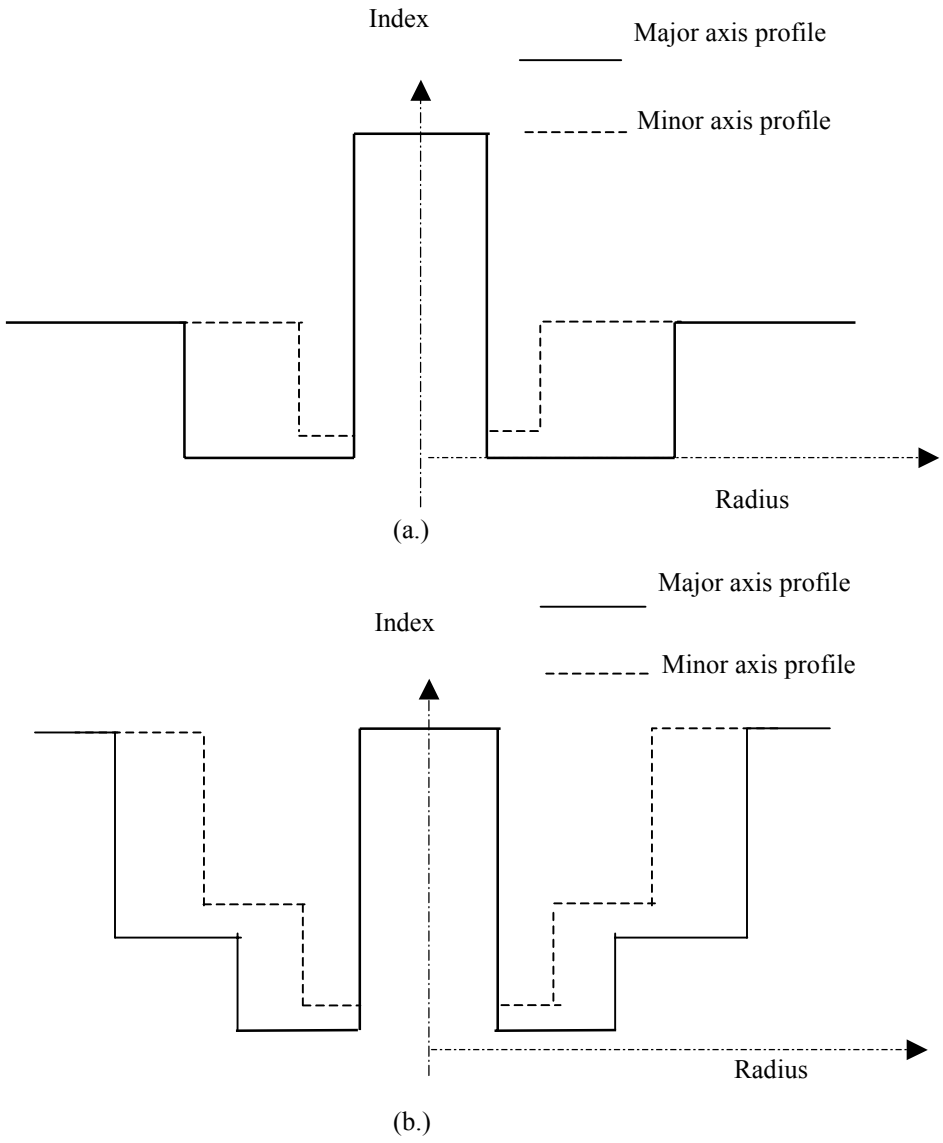

Figure 4.3: Index profiles of a three and four layer fiber polarizer. (a.) 3-layer polarizer (b.) 4-layer polarizer.

In Figure 4.3a the outer cladding is undoped fused silica, the inner cladding has been down doped with boron, and the core is up doped with germanium. In Figure 4.3b both the core and outer cladding are fused silica, while the first inner cladding has been doped with boron and the second inner cladding has been doped with flourine.

As seen from the preceding information, the W-type polarizer can be thought of as a highly birefringent W-fiber. The high birefringence causes each principal axis to have a distinctly different refractive index profile. From the information presented in

Chapter 3, one can see that if the profile of each axis meets the correct parameters, modes aligned along each axis will be cutoff at different wavelengths. Thus using the infinite

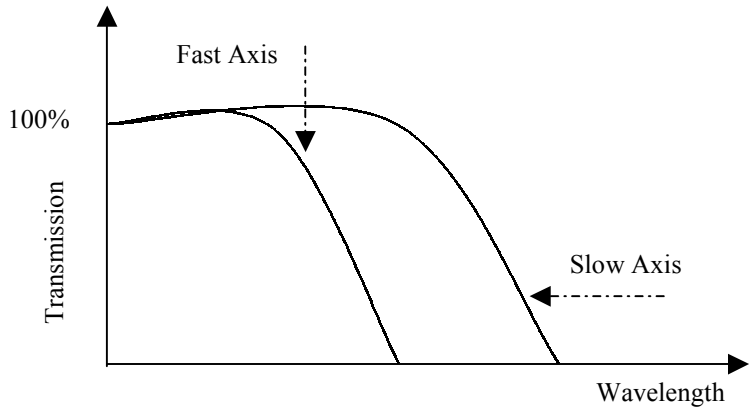

Figure 4.4: Ideal W-type fiber polarizer response.

cladding argument, modes along the axis with the short cutoff wavelength will begin to experience high radiation loss while the modes along the other axis propagate with relatively little loss. Figure 4.5 shows the ideal spectral response of a W-type polarizer. In the above figure, the slow and fast axis curves represent the spectral responses of the polarizer's principal axes. As can be seen the mode power along the fast axis is highly attenuated at short wavelengths, while the mode power along the slow axis propagates with relatively little loss. The bandwidth of the polarizer as defined by Messerly *et al* [29] is the wavelength range over which the power along the fast axis is attenuated by more than 25 dB and the power along the slow axis is attenuated by less than 1 dB. For maximum performance, the slope of the fast axis loss should be as steep as possible.

4.3 Summary of Problems with W-type Polarizers

This section discusses some of the problems in fully understanding the W-type polarizers and some of the anomalies observed in their spectral responses. From a theoretical standpoint, the physical shape of the polarizer presents problems in generating an appropriate eigenvalue equation to find the modal propagation constants. Not only do the fiber dimensions no longer have circular symmetry but the symmetry of the index profile is broken also. Scans of the refractive index profile of these fibers (provided by Bell Laboratories) reveal that in most samples the index of the core and inner claddings is

not uniform. Techniques are available for the analysis of these types of fibers [30] [31], but are much more complex than the methods shown in Chapter 2. In addition, based on what was shown in Chapter 3, a theoretical analysis of a type of fiber may not reveal all of its subtle characteristics.

Another short-coming of the W-type polarizer becomes clear when measurements are made of its spectral response. To measure the spectral response of a polarizer, the setup shown in Figure 4.5 is used. A white light source is focused onto a calcite crystal polarizer, which is focused onto the end section of the fiber polarizer. The output of this fiber is passed to a SM fiber that is connected to an OSA. The calcite polarizer produces linearly polarized light and as it is rotated, the maximum and minimum transmission of the fiber polarizer can be found. The maximum and minimum transmissions occur when light is launched along the slow and fast axis of the fiber polarizer.

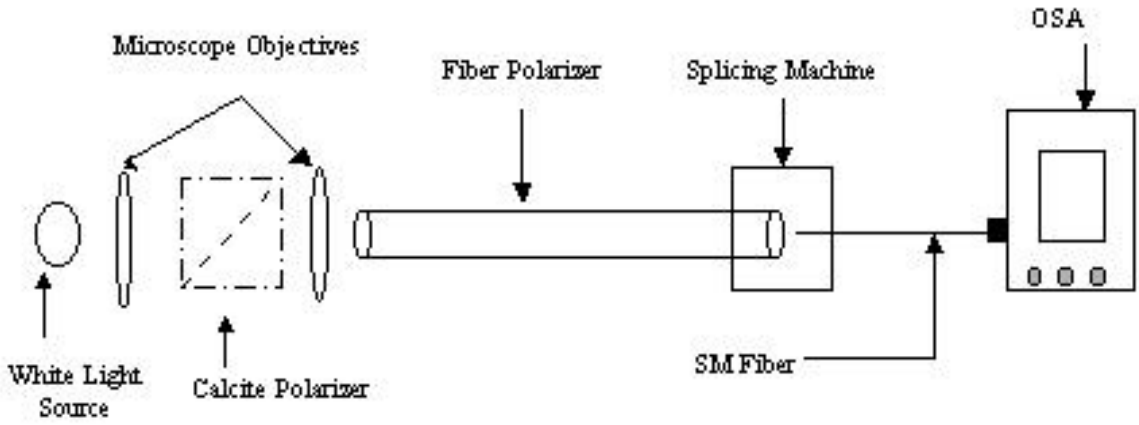

Figure 4.5: Experimental setup for measuring the spectral response of a W-type fiber polarizer.

The spectral responses of several samples of W-type fiber polarizers were measured. In these measurements, typical anomalies were revealed in the spectral plots. Figure 4.6 shows the spectral responses of two different 3-layer fiber polarizers. The spectrum in Figure 4.6a comes from a 24 cm sample and the spectrum in Figure 4.6b is from a 42 cm sample. In both cases an anomalous bit of power shows up in the scan of the fast axis. This extra bit of power greatly diminishes the polarizer's usable bandwidth, (the bandwidth of a polarizer is defined as the spectral rang over which the fast axis is attenuated by at least 25 dB and the slow axis is attenuated by less than 1 dB [29]. In

addition, the loss with respect to wavelength for the fast axis is not ideal. The power in the fast axis tends to taper off rather than have a nice sharp loss curve. The response of other polarizers did not even show a different response for light polarized along the slow and fast axes. In these cases, light along both axes suffered a high amount of loss.

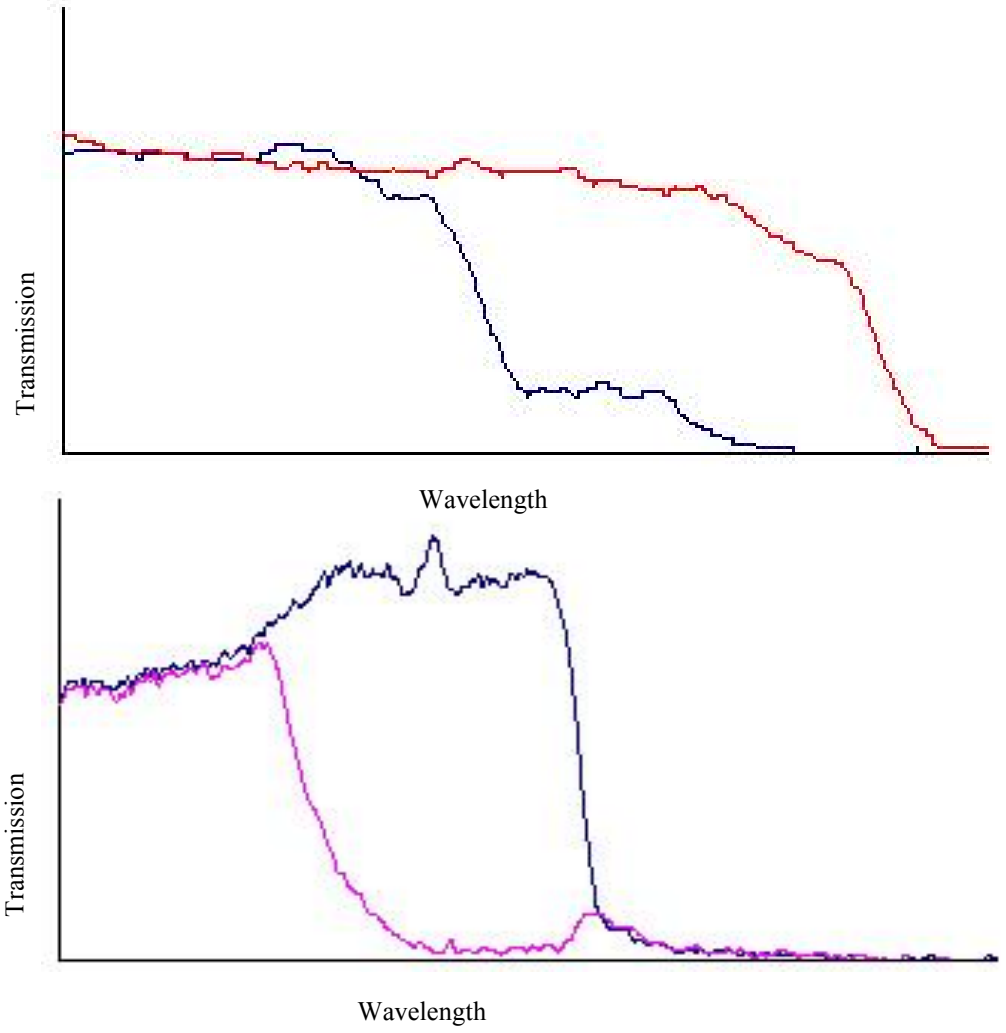

Figure 4.6: Spectral responses of W-type polarizers showing anomalous structure.

Since the actual spectral response of many of the fiber polarizers is not ideal, an important next step is to understand how these non-ideal characteristics can be changed. If experimental results can point to the source of unwanted characteristics in the fiber polarizers, it should be able to design better polarizers in the future.

4.4 Experimental Results

This section summarizes the results from experiments performed on the fiber polarizers. The main type of experiment is an index matching experiment. Fiber polarizers were coated with glycerin to match the index of their outer cladding and changes in their spectral responses were measured.

The procedure of the index matching experiments with fiber polarizers was very similar to the procedure used for W-fibers in Chapter 3. The response of a polarizer was measured and then its coating was completely removed. The fiber was then coated with glycerin and the spectral measurement was repeated. As with the W-fibers, the fiber polarizers were laid straight for all of the measurements. This was done to make sure that there were not any twists or bends in the fiber that would affect the spectrum.

Figures 4.8 and 4.9 show the results of two index matching experiments. In Figure 4.8a, the original spectral response of a 69 cm fiber polarizer is shown. The fast axis spectral response clearly shows an anomalous bump at approximately 975 nm. In Figure 4.8b, the same spectral response is shown, but now the response of the fast axis after the fiber has been index matched is included. It can be seen from the index matched curve that the fast axis cutoff slope is sharper and the anomalous bump has been suppressed. At point A, the amount of the power in the fast axis relative to the power in the slow axis, decreased from 34.6% to 8.5%. The index matching had a negligible effect on the spectral response of the slow axis. Figure 4.9a shows the original response of 42 cm sample of fiber polarizer and Figure 4.9b shows the original responses of the slow and fast axis along with the response of the fast axis when the fiber has been index matched. Again, coating the polarizer with glycerin with the appropriate refractive index value improves the polarizer's spectral characteristics. At point A on the graph in Figure 4.8b, the amount of power in the fast axis relative to the slow axis changed from 40.2% to 14.5% after the fiber was index matched. Again, the matching did not have any effect on the response of the slow axis.

As the above data shows, the width of the outer cladding of a W-type fiber polarizer has an effect on its spectral characteristics. This suggests that the performance of these devices can be improved by making their cladding larger. However, some index matching experiments did not have a significant effect on the polarizer's characteristics.

In the cases where there was not a significant improvement or change in the fiber's performance, the polarizer already had a worse response than the ones shown above. Therefore, there is probably not a universal solution to enhancing the W-type polarizer's performance.

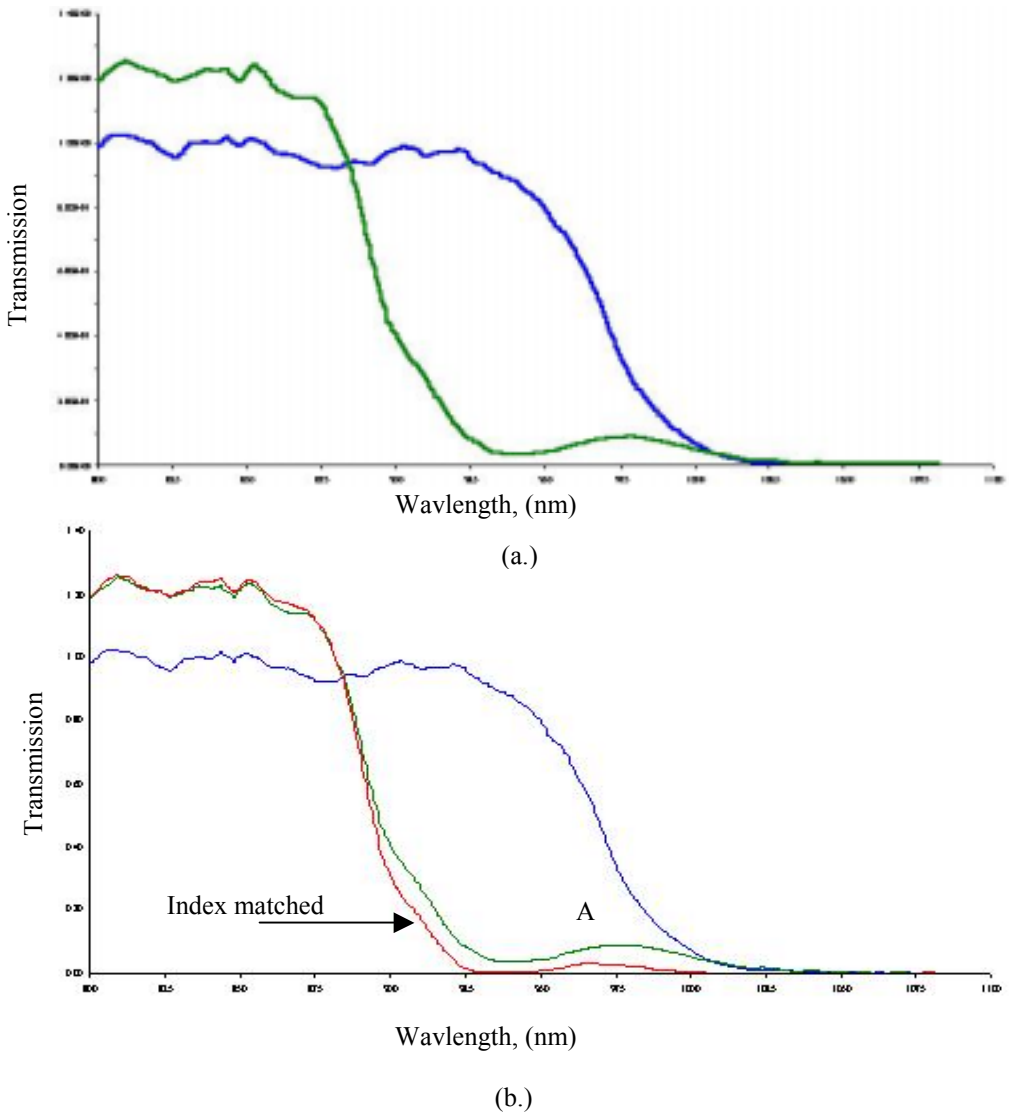

Figure 4.7: Spectral response of a 69 cm fiber polarizer. (a.) Original responses of the slow and fast axes (b.) Original responses and the fast axis response after the polarizer was index matched.

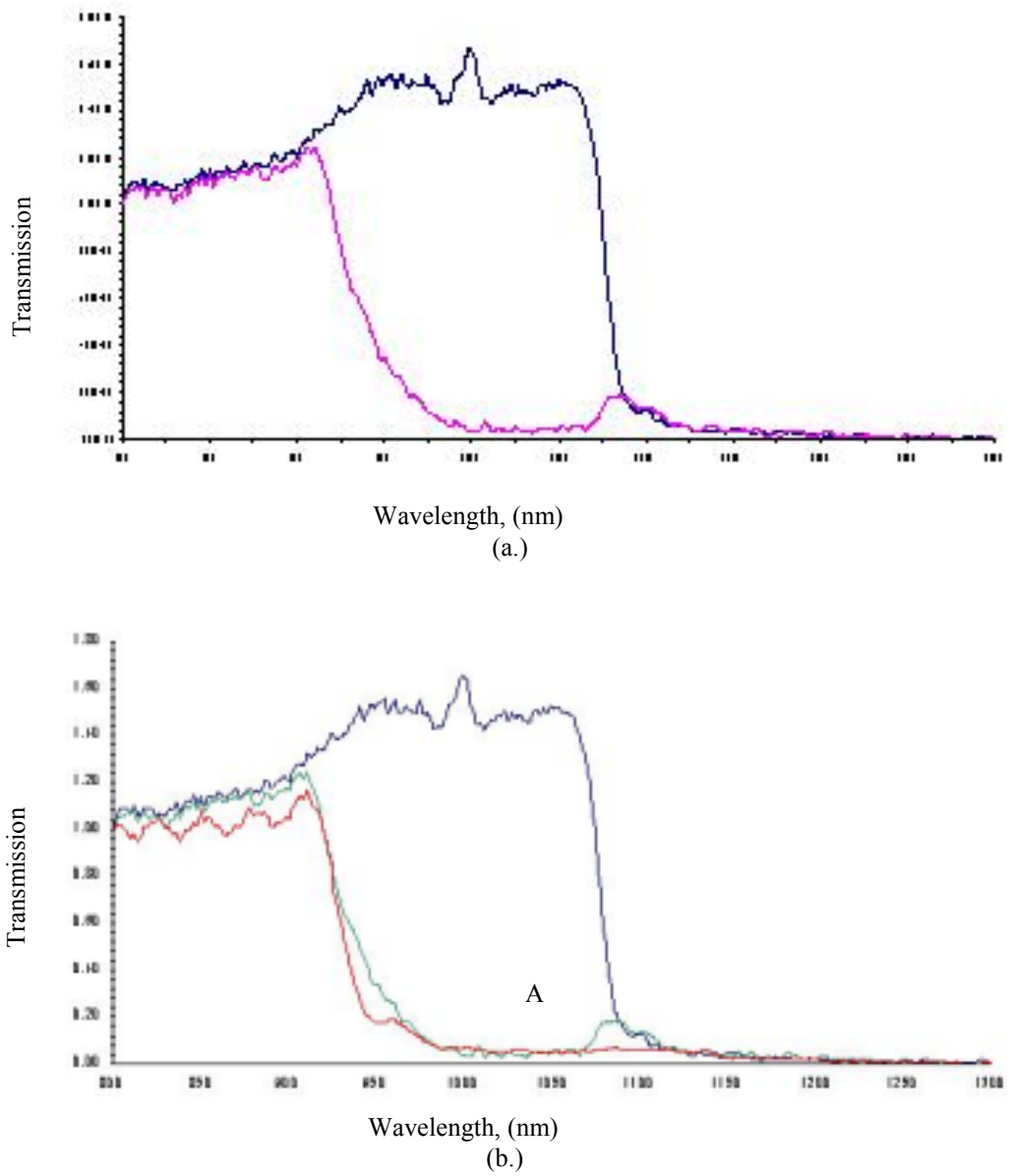

Figure 4.8: Spectral response of a 69 cm fiber polarizer. (a.) Original responses of the slow and fast axes (b.) Original responses and the fast axis response after the polarizer was index matched..

Chapter 5

Conclusions

7.1 Conclusions

This thesis reviewed the characteristics of W-fibers and W-type fiber polarizers. W-fibers were studied in depth both analytically and experimentally. It was determined that the traditional model of an infinite cladding can not be accurately applied to a W-fiber when it is operated at wavelengths longer than the cutoff wavelength of the fundamental mode. A more appropriate model of the W-fiber after cutoff is the supermode model. In this model, W-fiber modes are modes of the entire finite fiber cross-section and the anomalous loss peaks are explained in terms of absorption and scattering by the lossy fiber coating. Experimental results clearly support this model as do results from a numerical computer simulation.

W-type fiber polarizers were presented as a special type of highly birefringent W-fiber. The output of the polarizers is linearly polarized along one of the fiber's principal axes. However, measurements revealed that distortions appeared in some of the polarizers' spectra and some polarizers did not appear to polarize at all. Experiments showed that if the polarizer is coated with an index matching oil, its performance as a polarizer improves. However, this improvement is not universal and therefore some samples of the W-type polarizer have other issues to be addressed.

7.2 Suggestions for Future Work

The analysis and results presented here clarifies issues concerning the operation of W-fiber and W-type fiber polarizers. From this work several new areas of investigation can be undertaken.

Most importantly, new W-fiber preforms should be made and drawn into fibers. W-fibers made with known refractive index profiles can be put through a battery of tests (spectral response, index matching, etc.). Results from these tests can be compared to computer simulations in order to further verify the accuracy of the supermode model.

Next, a computer model can be generated for the W-type polarizers based on results of the experiments with the W-fibers. If an accurate model can be made, it should be possible to pinpoint problems in the existing polarizers and create new polarizers with acceptable operating characteristics.

Works Cited

1. Hecht, J., *Optics*. 3 ed. 1998, New York: Addison Wesley Longman Inc. 694.
2. Simpson, J.R., *et al.*, *A Single-Polarization Fiber.* Journal of Lightwave Technology, 1983. **LT-1**(2): p. 370 - 373.
3. Kawakami, S. and S. Nishida, *Characteristics of a Doubly Clad Optical Fiber with a Low-Index Inner Cladding.* IEEE Journal of Quantum Electronics, 1974. **QE-10**(12): p. 879 - 887.
4. Okoshi, T., *HETERODYNE AND COHERENT OPTICAL FIBER COMMUNICATIONS - RECENT PROGRESS.* IEEE Transactions on Microwave Theory and Techniques, 1982. **30**(8): p. 1138 - 1149.
5. Kajioka, H. and H. Matsumura, *SINGLE POLARIZATION OPTICAL FIBER AND ITS APPLICATIONS.* Hitachi Review, 1984. **33**(4): p. 215 - 218.
6. Falquier, D., *et al.*, *Basis for a polarized superfluorescent fiber source with increased efficiency.* Optics Letters, 1996. **21**(23): p. 1900 -1902.
7. Agrawal, G.P., *Fiber Optic Communication Systems*. 2nd ed. Microwave and Optical Engineering, ed. K. Change. 1997, New York: John Wiley and Sons, Inc.
8. Snyder, A.W. and J.D. Love, *Optical Waveguide Theory*. 1983, New York: Chapman and Hall. 734.
9. Synder, A.W., Transactions of Microwave Theory Techniques, 1969. **MTT-17**: p. 1130.
10. Monerie, M., *Propagation in Doubly Clad Single-Mode Fibers.* IEEE Journal of Quantum Electronics, 1982. **QE-18**(4): p. 535 - 542.
11. Sammut, R.A., *Range of monomode operation of W-fibres.* Optical and Quantum Electronics, 1978. **10**: p. 509 - 514.
12. Cohen, L.G., D. Marcuse, and W.L. Mammel, *Radiating Leaky-Mode Losses in Single-Mode Lightguides with Depressed-Index Claddings.* IEEE Journal of Quantum Electronics, 1982. **QE-18**(10): p. 1467 - 1472.
13. Buck, J.A., *Fundamentals of Optical Fibers*. 1995, New York: John Wiley and Sons. 264.
14. Sansonetti, P., *et al.*, *Evidence of Fundamental Mode Cutoff in Depressed Inner Cladding Single-Mode Fibers.* Electronics Letters, 1982. **18**(23): p. 989-991.
15. Dalton, M., *Glycerol*. 1953: Reinhold Publishing Company.

16. Francois, P.L. and C. Vassallo, *Finite cladding effects in w-fibers: a new interpretation of leaky modes.* Applied Optics, 1983. **22**(19): p. 3109 - 3120.

17. Henry, W.M., J.D. Love, and G.D. Peng, *Anomalous loss in depressed-cladding and W-fibres.* Optical and Quantum Electronics, 1993. **25**: p. 409 - 416.

18. Shah, V. and L. Curtis, *Mode Coupling Effects of the Cutoff Wavelength Characteristics of Dispersion-Shifted and Dispersion-Unshifted Single-Mode Fibers.* Journal of Lightwave Technology, 1989. **7**(8): p. 1181 - 1186.

19. Renner, H., *Leaky-Mode Loss in Coated Depressed-Cladding Fibers.* IEEE Photonics Technology Letters, 1991. **3**(1): p. 31 - 32.

20. Tomita, A. and D. Marcuse, *Mode Coupling Loss in Single-Mode Fibers with Depressed Inner Cladding.* IEEE Journal of Lightwave Technology, 1983. **LT-1**(3): p. 449 - 452.

21. Steblina, V.V., *et al.*, *Cladding mode degeneracy in bent W-fibers beyond cutoff.* Optics Communications, 1998. **156**: p. 271 - 274.

22. Besley, J.A. and J.D. Love, Optoelectronics, IEEE Proceedings, 1997. **144**(6): p. 411 - 19.

23. Safaai-Jazi, A. and C.J. Chang. *Analysis and Design of a Narrow All-Fiber Spectral Filter Made of Step-Index and W-type fibers*, IEEE Proceedings - Southeastcon, Session 12C-1, 1989

24. Stolen, R.H., W. Pleibel, and J.R. Simpson, *High-Birefringence Optical Fibers by Preform Deformation.* Journal of Lightwave Technology, 1984. **LT-2**(5): p. 639 - 641.

25. Tajima, K., M. Ohashi, and Y. Sasaki, *A New Single-Polarization Optical Fiber.* Journal of Lightwave Technology, 1989. **7**(10): p. 1409 - 1502.

26. Bergh, R.A., H.C. Lefevre, and H.J. Shaw, *Single-mode fiber-optic Polarizer.* Optical Society of America, 1980. **5**(11): p. 479 - 80.

27. Morishita, K. and K. Aso, *Fiber Loop Polarizers Using a Fused Taper Coupler.* Journal of Lightwave Technology, 1994. **12**(4): p. 634 - 37.

28. Rashleigh, S.C. and R.H. Stolen, *Preservation of Polarization in Single-Mode Fibers.* Optical Society of America, Invited talk.

29. Messerly, M.J., J.R. Onstott, and R.C. Mikkelson, *A Broad-Band Single Polarization Optical Fiber.* Journal of Lightwave of Technology, 1991. **9**(7): p. 817 - 820.

30. Skinner, I.M., *Simple Approximation Formulae for Elliptical Dielectric Waveguides.* Optical and Quantum Electronics, 1986. **18**: p. 345 - 354.

31. Kalosha, V.P. and A.P. Khapalyuk, *Polarization Characteristic Calculation of Three-Layer Elliptical Single-Mode Fibres.* Optical and Quantum Electronics, 1985. **17**: p. 253 - 261.

Vita

Corey Paye was born in Baltimore, Maryland. After graduating from Baltimore Polytechnic Institute, he attended the Florida Institute of Technology. In 1998 he graduated with honors with a B.S. in Electrical Engineering. In 2001 he completed his M.S. degree in Electrical Engineering at Virginia Polytechnic Institute and State University. Corey is an avid reader and enjoys homebrewing.